

https://dspace.org/

The Design of DiscreteTime Systems With Prescribed Probability Distribution and Power Spectrum Poles

André McDonald; Michael Van Wyk; JACQUES ÉTIENNE CILLIERS

https://hdl.handle.net/10539/45523
WOS

Downloaded from a DSpace repository. https://dspace.org/

IEEE Access
Multidisciplinary | Rapid Review | Open Access Journal

Received 8 March 2025, accepted 29 March 2025, date of publication 9 April 2025, date of current version 21 April 2025.

Digital Object Identifier 10.1109/ACCESS.2025.3558799

RESEARCH ARTICLE

The Design of Discrete-Time Systems With Prescribed Probability Distribution and Power Spectrum Poles

ANDRÉ MARTIN MCDONALD[1,2], (Member, IEEE), MICHAËL ANTONIE VAN WYK[2,3], (Senior Member, IEEE), AND JACQUES ÉTIENNE CILLIERS[1,4]

[1]Defence and Security Cluster, Council for Scientific and Industrial Research, Pretoria 0184, South Africa
[2]School of Electrical and Information Engineering, University of the Witwatersrand, Johannesburg 2000, South Africa
[3]Department of Electrical Engineering, City University of Hong Kong, Hong Kong, SAR, China
[4]Radar and Electronic Warfare Centre of Excellence, EDGE Group, Abu Dhabi, United Arab Emirates

Corresponding author: André Martin McDonald (amcdonald@csir.co.za)

This work was financially supported in part by the Carl and Emily Fuchs Foundation's Chair in Systems and Control Engineering, University of the Witwatersrand, South Africa.

ABSTRACT This paper addresses the problem of designing nonlinear discrete-time dynamical systems for prospective use in low-complexity random signal generators. Drawing upon ergodic systems theory, we derive a novel method for designing nonlinear systems with zero-input responses that simultaneously satisfy two user-specified statistical metrics as specifications. These metrics are a piecewise-constant probability density function and a power spectral density expressed as a rational function with an arbitrary number of prescribed non-repeating poles. This new method configures a memoryless nonlinearity (i.e., a map) with a low-complexity hat-like structure as a recursive system with adjustable parameters, thereby yielding a simplified and explicit relationship between the system's parameters and the statistical metrics of its response. This yields a matrix design approach that, unlike existing methods, affords the freedom to prescribe all of the poles as a set of non-repeating complex values without resorting to a numerical search over the parameter space for a candidate solution. Simulations are presented of elementary systems constructed using the novel method, and the link between the maps' structure and the observed statistical behavior is expounded. More sophisticated systems with richer statistical metrics are constructed as examples that demonstrate the method's versatility. We also demonstrate the independent adjustment of the center frequency and bandwidth of power spectrum modes during system design, which affords greater freedom than existing methods to select the power spectral density. We anticipate that the proposed method will find application in the construction of efficient random signal generators for Monte Carlo simulation in domains such as mobile communications, radar engineering, data encryption and optimization.

INDEX TERMS Discrete-time system, inverse Frobenius-Perron problem, Markov map, nonlinear system modeling, power spectral density, random number generation, random signal generation.

NOMENCLATURE

ACF	Autocorrelation function.
DRFM	Digital radio frequency memory.
FPM	Frobenius-Perron matrix.
FPO	Frobenius-Perron operator.
IFPP	Inverse Frobenius Perron problem.
MAS	Multi-agent system.
PDF	Probability density function.
PSD	Power spectral density.
PWC	Piecewise-constant.
PWL	Piecewise-linear.
StIEP	Stochastic inverse eigenvalue problem.
UAV	Unmanned aerial vehicle.

The associate editor coordinating the review of this manuscript and approving it for publication was Ludovico Minati.

© 2025 The Authors. This work is licensed under a Creative Commons Attribution-NonCommercial-NoDerivatives 4.0 License.
For more information, see https://creativecommons.org/licenses/by-nc-nd/4.0/

I. INTRODUCTION

The simulation of natural and artificial phenomena is an important component of scientific investigation and engineering [1]. In these domains, *random signal generators* are used to simulate processes that are not fully predictable and modeled from observed statistics. These generators are required to produce pseudorandom signals with prescribed statistical metrics, such as the signals' probability density function (PDF) and power spectral density (PSD) [2], [3], [4], [5], [6].

It became widely known in the 1970s that dynamical systems with unsophisticated evolution rules are not excluded from generating a zero-input time response with rich dynamics and statistical behavior [7]. These systems hold promise as highly efficient random signal generators for simulating diverse processes with distinct statistical characteristics [8], [9]. In this application, the system has to be designed such that almost every zero-input response, as generated by selecting a distinct initial system state, satisfies the prescribed statistical metrics. This design problem, referred to as the *inverse Frobenius-Perron problem* (IFPP) [10], has been studied within the probabilistic modeling community since the 1970s. However, the IFPP has not yet been fully solved.

The IFPP requires the design of a discrete-time, one-dimensional dynamical system that is (i) ergodic and (ii) generates a real-valued zero-input response that satisfies prescribed statistical metrics [10]. Within the context of the IFPP, the system is constrained to a recursive configuration of a single memoryless nonlinearity or *map*. Several formulations of the IFPP, each specifying different statistical metrics for the system's response, have emerged in the literature [11], [12], [13], [14].

The original formulation of the IFPP, labeled IFPP-I, prescribes the PDF of the system's zero-input response [11]. Although systems designed as solutions to IFPP-I have been successfully applied as random signal generators (recent examples are [15], [16], [17], [18]), these systems lack the characteristics required for random signal generation in *Monte Carlo simulations*. These simulations involve more sophisticated phenomena and require the specification of additional statistical characteristics for the signals. This is evident in Monte Carlo simulations of mobile communications and radar systems.

In mobile communications systems, the fading characteristics of the received signal have a major impact on system performance [19]. Recent work addresses the simulation of realistic fading signals for these systems [20], [21]. Monte Carlo performance evaluation in this domain requires random signals with a particular PDF and a PSD selected from one of several models developed for multipath radio channels [22]. Generators that only permit selection of the signals' PDF cannot be used in this context.

In radar engineering, *digital radio frequency memory* (DRFM) systems for evaluating the performance of radar systems are gaining popularity [23], [24], [25], [26], [27]. DRFM systems operate within the hardware loop and are required to generate realistic pseudorandom signals that mimic the radar's environment. These signals must be generated at very high sample rates of up to 5 gigasamples per second. In radar environments, multipath propagation [28], clutter [29], [30], [31] and fluctuating targets [32], [33] affect system performance and yield return signals with Doppler spectra of different shapes. DRFM systems thus rely on efficient random signal generators that afford as much freedom as possible to prescribe the signals' PDF and PSD.

Recently, random signal generators with specifiable statistical characteristics have found application in the modeling and simulation of uncrewed aerial vehicles (UAVs).. In [34], random signal generators that make use of chaotic maps with a selectable mean value were used to generate unpredictable flight paths for UAVs that perform surveillance. Random signal generators were also used to generate correlated noise for simulating vibration in UAVs [35] and to evaluate control methodologies applied in this context [36].

The need for more realistic system models and efficient random signal generators with greater versatility has attracted interest to formulations of the IFPP that specify additional statistical metrics for the system [10]. One such formulation, labelled IFPP-II, requires the design of a system with a zero-input response that simultaneously possesses a prescribed PDF *and* PSD (or equivalently, by the Wiener-Khinchin theorem [37], a prescribed *autocorrelation function* or ACF) as specifications [12]. This design problem is significantly more complicated than IFPP-I due to the elementary structure of the system configuration prescribed by the IFPP. More specifically, the memoryless nature of the map and the absence of filters in the system configuration prescribed by the IFPP affords little design freedom to directly manipulate the dynamics of the system's zero-input response, and thereby shape the response PSD.

Groundbreaking work towards solving IFPP-II has been carried out, but the methods developed [12], [38], [39], [40], [41] are of limited practicality. In general, methods aimed at solving IFPP-II define a class of candidate systems, such that each system is fully specified by a large set of parameters that define the underlying map's branch functions. IFPP-II is then reformulated as the problem of selecting a point in the parameter space that yields a system with the desired statistical metrics. If the relationship between the parameters and statistical metrics of the candidate systems is of excessive complexity, a direct analytical approach to parameter selection cannot be formulated. This led to the development of numerical methods that rely on a search over the parameter space for a system that meets the requirements [38], [39]. However, due to the high dimensionality of the search space, the time required to perform the search is impractical and convergence to a solution cannot be guaranteed. Another disadvantage of numerical methods is a lack of theory on the class of PSDs that are realizable.

Constraints may be enforced on the structural characteristics of the candidate systems' maps to yield simplified expressions for their statistical metrics as functions of

the underlying maps' branch function parameters. These expressions permit the formulation of analytical methods for selecting the parameters to satisfy prescribed statistical metrics [12], [40], [41]. Although these analytical methods are immune to numerical problems such as non-convergence, the structural constraints imposed on the candidate maps generally restrict the class of statistical metrics that are realizable. Examples include PSDs restricted to a single mode [12] and response PDFs that are piecewise constant (PWC) [40], [41].

The work presented in this paper addresses limitations of a more recent analytical method [40] aimed at solving IFPP-II. The candidate systems of this method comprise the piecewise-linear (PWL) *semi-Markov maps*, which are constrained to map intervals from a finer domain partition onto the intervals of a rougher Markov domain partition. This constraint permits matrix representations of the system's *Frobenius-Perron operator* (FPO), which governs the evolution of state density functions under iteration of the map. We distinguish between two such matrices, referred to as the *order-zero* and *order-one Frobenius-Perron matrices* or FPMs. These matrices characterize the evolution of state density functions that are PWC and PWL over the Markov partition, respectively.

The relevant statistical metrics of the above systems are functions of their order-zero and order-one FPMs. More specifically, the response PDF is PWC over the Markov partition and coincides with the maximal eigenvector of the order-zero FPM. The response PSD is expressed as a rational function, such that its poles coincide one-to-one with the unique nonzero and nonunity (in magnitude) eigenvalues of the order-one FPM.[1] This implies a multimodal PSD where each mode's bandwidth and center frequency (referred to here as the *mode characteristics*) coincide with the modulus and argument of a distinct eigenvalue of the order-one FPM, respectively.

The elements of order-zero and order-one FPMs are unsophisticated functions of the underlying map's branch function parameters. This permits analytical matrix-based methods for system design. The method of [40] follows a three-step design approach. First, the method constructs a candidate order-zero FPM with selectable real eigenvalues. Second, a map is constructed to be consistent with the candidate order-zero FPM; this is labelled the *original map*. In the final step, the method constructs a second map as a *topological conjugate* of the original map, and configures this conjugate map as the recursive system. The final step yields a response PDF that is a PWC approximation of a prescribed smooth density function. The method also permits selection of a *proper* subset of poles in the response PSD as non-repeating real values. These poles coincide with the distinct eigenvalues selected for the candidate order-zero FPM.[2]

The method of [40] allows for the prescription of spectral mode characteristics through the selection of power spectrum poles. However, the modes and characteristics that are prescribable using this method are restricted, which in turn limits the designer's freedom to select the response PSD. In particular, the method necessarily yields PSDs with one or more unselectable poles that manifest as additional and unwanted spectral modes. Although systems with an arbitrary number of poles may be constructed, the selectable poles are limited to real values only. This restricts the corresponding spectral modes to be centered only at zero or π radians per sample.

This paper proposes a novel analytical method for designing a system with a zero-input response that satisfies prescribed statistical metrics. The novel method, which follows the same three-step design approach as [40], permits the simultaneous prescription of the poles for the response PSD as well as the response PDF as a piecewise-constant function. However, it improves upon existing methods by affording the freedom to *arbitrarily select* the number of PSD poles and to prescribe *all* of these poles as a set of non-repeating *complex values*, thereby allowing the designer to select arbitrary center frequencies for the spectral modes. This greater flexibility permits the designer to more closely approximate power spectra specified in Monte Carlo simulations, thereby facilitating more accurate simulation results when using the novel systems as efficient random signal generators.

The following two challenges were encountered in developing the novel analytical method. First, to permit the selection of all power spectrum poles as complex values, the novel method for system design requires an analytical means for designing a candidate order-zero FPM such that all eigenvalues of the matrix may be prescribed as complex values by the designer. The first contribution of this paper addresses this challenge by using the authors' recent analytical solution to the inverse eigenvalue problem [43] to construct the candidate order-zero FPM as a *stochastic matrix* (i.e., a nonnegative matrix with columns that sum to unity) in the first design step.[3] This solution yields an order-zero FPM of arbitrary dimensionality and with selectable *complex* eigenvalues. In turn, this yields a response PSD with an arbitrary number of modes and, unlike the method of [40], permits the prescription of arbitrary mode center frequencies from the interval $\omega \in [-\pi, \pi)$.

Second, the novel method for system design requires a mechanism for preventing the manifestation of unselectable poles in the PSD of the system response. As these unwanted poles coincide with those eigenvalues of the order-one

[1] It can be shown that each eigenvalue λ of any ergodic system's order-one FPM necessarily satisfies $|\lambda| \leq 1$; refer to [42].

[2] It is shown in section II that the order-zero FPM is a submatrix of the larger order-one FPM, and that all eigenvalues of the order-zero FPM necessarily appear in the eigenspectrum of the order-one FPM.

[3] Stochastic matrices are widely used in the systems and control domains; see, for example, [44] and [45].

FPM that are not shared with the order-zero FPM, they cannot be suppressed solely via selection of the order-zero FPM. The only remaining freedom that may be utilized to suppress unwanted poles is the selection of the map in the second design step. However, designing a map with branch features that suppress unwanted poles is a non-trivial problem.

The above challenge is resolved by the novel contribution of an algorithm for constructing and configuring a *hat map* as the recursive system that satisfies the candidate order-zero FPM. First investigated in [39], the hat maps have PWL branch functions and are defined such that the left and right branches of each consecutive pair of neighboring branches have a positive and negative slope of equal magnitude (the name of these maps arises from the hat-like appearance of the branch pairs). In this paper, it is proved analytically and demonstrated using numerical examples that the structural features of these maps prevent the manifestation of unwanted spectral modes with characteristics that cannot be prescribed by selecting the order-zero FPM eigenvalues. More specifically, it is shown that the symmetry of each branch pair forces the eigenvalues of the order-one FPM that are not shared with the order-zero FPM to zero, thus preventing their appearance as power spectrum poles.

As a result of the contributions outlined above, the novel method permits the design of systems with PSDs that comprise an arbitrary and selectable number of modes, such that each mode's center frequency may be selected and its bandwidth adjusted. Unlike the existing method of [40], no unwanted spectral modes appear in the PSD, and the mode center frequencies may be selected without restriction. This grants the designer greater freedom to specify the power spectrum, and thus yields a more practical and versatile simulation tool. Unlike the numerical methods of [38] and [39], the proposed method is fully analytical, thereby excluding numerical problems such as non-convergence and allowing for the derivation of expressions that qualify a candidate collection of power spectrum poles as realizable. However, the novel method does not afford the opportunity to select the zeros of the PSD, thus excluding the realization of arbitrary rational power spectra. Furthermore, the PDF of the system's response is a PWC function, and can thus only approximate an arbitrary prescribed density function that is smooth. These limitations are shared by the existing method of [40].

We demonstrate the novel method by constructing examples of elementary systems that possess PSDs with one and two prescribed poles. These PSDs are plotted and characterized using pole-zero plots, and the structural properties of each system's map that give rise to the observed spectral characteristics are identified and described. The novel method is then used to construct examples of more sophisticated systems that demonstrate its versatility. These systems generate a zero-input response with a PDF that approximates the beta density function and PSDs with more than two prescribed poles. The statistical behavior of all the systems constructed as examples are verified using numerical simulation.

The design and performance evaluation of random signal generators that incorporate systems constructed using the novel method are not addressed in this paper. However, we observe that the PWL nature of these systems' maps permits random signal generation with low computational complexity. In particular, it was demonstrated in numerical experiments that a software implementation of recursive systems with PWL semi-Markov maps has lower memory requirements and achieves a reduction of up to 22% in the average computing time required to generate random signals, as compared to conventional random signal generators [9]. Due to the richness of their power spectra and the simplicity of their evolution rules, it is anticipated that systems designed using the new method will find use in applications that require versatile yet efficient random signal generators.

The remainder of this paper is set out as follows. Section II presents necessary mathematical background on the probabilistic characterization of one-dimensional dynamical systems and the semi-Markov maps. A review of previous methods aimed at solving IFPP-II is presented in section III. Section IV outlines the novel method, presents the theory underlying each of its steps and introduces the class of hat maps. The elementary and more sophisticated systems constructed using the novel method are characterized in sections V and VI, respectively. Conclusions and topics for future work are presented in sections VII and VIII, respectively.

II. MATHEMATICAL BACKGROUND

In this section, the system configuration prescribed by the IFPP, and the relevant statistical metrics of the system's zero-input response, are defined. Thereafter, the class of piecewise-monotonic maps is defined, and the theory necessary for the probabilistic characterization of these maps is presented. The section concludes with the definition and characterization of the semi-Markov maps, which form a subclass of the piecewise-monotonic maps. These semi-Markov maps are designed and configured as systems by the novel method proposed in this paper. The material presented in this section was adapted from earlier articles by McDonald et al. [10], [44].

A. SYSTEM DEFINITION

Grossman and Thomae [11] first defined the problem of designing a system with zero-input response that satisfies a prescribed PDF, which eventually became known as the IFPP. The discrete-time and one-dimensional dynamical system model proposed by [11] is presented in Fig. 1. This system model has subsequently been adopted as the standard system model for the IFPP by the research community (refer to the survey of [10]).

The system of Fig. 1 possesses a memoryless nonlinearity $S : \Omega \to \Omega$ as evolution rule. Here, the system's state space is denoted by $\Omega \triangleq [0, 1]$. Let v_t and x_t denote the system

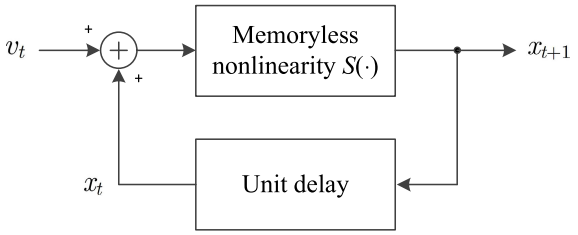


FIGURE 1. Diagram of a recursive, discrete-time and one-dimensional dynamical system configured to use the memoryless nonlinearity S as its evolution rule.

input and system state at time $t = 0, 1, \ldots$, where

$$v_t = \begin{cases} v \in \Omega, & \text{if } t = 0 \\ 0, & \text{if } t > 0, \end{cases} \tag{1}$$

and

$$x_{t+1} = \begin{cases} 0, & \text{if } t = -1 \\ S(x_t + v_t), & \text{if } t \geq 0. \end{cases} \tag{2}$$

The initial state of the system is given by $x_1 = S(v_0)$. The zero-input response[4] of the system then evolves independently according to $x_{t+1} = S(x_t)$, where $t \geq 1$.

We next define two statistical metrics, associated with the zero-input response of the system in Fig. 1, that are relevant to the IFPP considered in this paper. These statistical metrics are the PDF and ACF of the system's zero-input response. We present standard expressions from the literature for these metrics [11], [12]. In these definitions, it is assumed the system is ergodic [46], which implies that each metric is valid for almost every initial system state $x_1 \in \Omega$ [47].

The PDF f_S of the zero-input response is defined as the asymptotic density function [11]

$$f_S(x) = \lim_{\substack{\mu(I)\to 0 \\ I\to x}} \lim_{T\to\infty} \frac{1}{\mu(I)} \frac{1}{T} \sum_{t=0}^{T-1} \chi_I\big(S^t(x_1)\big), \tag{3}$$

where S^t denotes the t-fold composition of S with itself and $S^0(x) \triangleq x$. In this expression, I denotes a Borel set, μ denotes the Borel measure, and

$$\chi_I(x) \triangleq \begin{cases} 1 & \text{if } x \in I \\ 0 & \text{if } x \notin I. \end{cases} \tag{4}$$

The ACF ϕ_S of the zero-input response is defined as [12]

$$\phi_S(\tau) \triangleq \lim_{T\to\infty} \frac{1}{T} \sum_{t=0}^{T-1} S^t(x_1) S^{t+|\tau|}(x_1), \quad \tau \in \mathbb{Z}. \tag{5}$$

By the Wiener-Khinchin theorem [37], the PSD of the system's zero-input response is the frequency-domain representation of the corresponding ACF. Expressions for the PSDs associated with the systems considered in this paper are derived in section II-C.

[4]The system's zero-input response may alternatively be interpreted as its scaled (Kronecker) impulse response.

B. PIECEWISE-MONOTONIC MAPS

Let $\mathcal{Q}$ denote a partition $\mathcal{Q} = \{Q_1, Q_2, \ldots, Q_M\}$ of Ω, such that $Q_m = (q_m, q_{m+1})$ denotes the partition intervals and $P(\mathcal{Q}) = \{q_1, q_2, \ldots, q_{M+1}\}$ denotes the partition points, where $0 = q_1 < q_2 < \ldots < q_{M+1} = 1$ with integer $M > 1$. We restrict attention to the class of piecewise-monotonic maps $S \in \Gamma(\mathcal{Q})$.

Definition 1 (Class $\Gamma(\mathcal{Q})$): A surjective map $S : \Omega \to \Omega$ is piecewise monotonic [8] (i.e., $S \in \Gamma(\mathcal{Q})$) if there exists a partition $\mathcal{Q}$ of the unit interval such that

(i) each branch function $S_m \triangleq S|_{(q_m, q_{m+1})}$ is a C^r function, for some $r \geq 1$, that can be extended to a C^r function over $[q_m, q_{m+1}]$, and

(ii) $|S'_m| > 0$ for $m = 1, 2, \ldots, M$, where $S'_m \triangleq dS_m/dx$.

We consider an ergodic system, such that the PDF calculated over almost every zero-input response of the system coincides with the system's stationary density [46]. Thus, we characterize the system in a probabilistic sense. Let X_1 denote a real random variable on the probability space $(\Omega, \mathcal{B}, P_1)$, which represents the initial state of the system. Here, $\mathcal{B}$ denotes the Borel σ-algebra on Ω and P_1 is a probability measure. Since S is surjective and measurable on $\mathcal{B}$ [10], the random variables $X_2, X_3, \ldots$, defined by $X_{t+1} = S(X_t)$ for $t \geq 1$, have corresponding probability measures given by $P_{t+1}(B) = P_t(S^{-1}(B))$, $B \in \mathcal{B}$.

Let P_1 be absolutely continuous with respect to the Borel measure μ. The Radon-Nikodym theorem then implies the existence of a function $f_1 \in \mathcal{D}$ associated with X_1, where $\mathcal{D} \triangleq \{f \in L^1(\Omega) : f \geq 0 \text{ and } ||f|| = 1\}$ denotes the set of all PDFs on Ω. The density function f_1 satisfies $P_1(B) = \int_B f_1(x) d\mu(x)$ for all $B \in \mathcal{B}$. Since $S \in \Gamma(\mathcal{Q})$ is nonsingular with respect to μ [10], each measure P_t, where $t > 1$, is also absolutely continuous with respect to μ, and may be associated with a corresponding density $f_t \in \mathcal{D}$. The linear operator $\mathcal{P}_S : L^1(\Omega) \to L^1(\Omega)$, referred to as the FPO of S, characterizes the evolution of densities generated by the system (i.e., under iteration of S) according to the expression $f_{t+1} = \mathcal{P}_S f_t$ for $t \geq 1$. The FPO is uniquely defined by

$$\int_B (\mathcal{P}_S f)(x) d\mu(x) = \int_{S^{-1}(B)} f(x) d\mu(x), \quad B \in \mathcal{B}. \tag{6}$$

The FPO of a system possessing $S \in \Gamma(\mathcal{Q})$ as evolution rule has the explicit representation

$$(\mathcal{P}_S f_t)(x) = \sum_{m \in N(x)} \frac{f_t \circ S_m^{-1}(x)}{|S'_m \circ S_m^{-1}(x)|}, \tag{7}$$

where $N(x) \triangleq \{m : x \in S(Q_m)\}$ [8].

C. SEMI-MARKOV MAPS

We next introduce a subset of the piecewise-monotonic maps, referred to as the class of semi-Markov maps [48]. The structure of these maps permits matrix solutions to the IFPP. Semi-Markov maps are defined over a two-level hierarchy of partitions. Let $\mathcal{Q}$ denote a partition of the unit interval as before (referred to as the *Markov partition*),

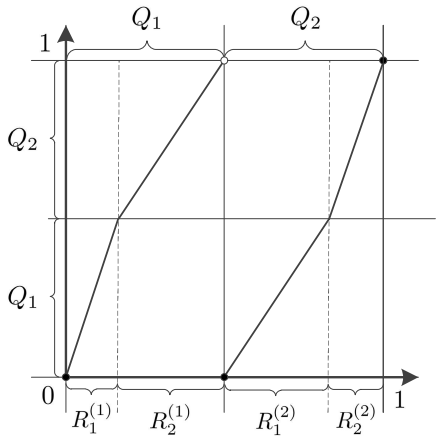


FIGURE 2. An example of an $\mathcal{R}(\mathcal{Q})$-semi-Markov map [44].

and let the nonempty set of open intervals $\mathcal{R}^{(m)} \triangleq \{R_1^{(m)}, R_2^{(m)}, \ldots, R_{c(m)}^{(m)}\}$ constitute a partition of the closure of Q_m for each $m = 1, 2, \ldots, M$. We refer to the unit-interval partition $\mathcal{R} = \{R_j^{(m)}\}, m = 1, 2, \ldots, M$ and $j = 1, 2, \ldots, c(m)$, as a *sub-partition* of $\mathcal{Q}$. The $\mathcal{R}(\mathcal{Q})$-semi-Markov maps are then defined as follows (an example is plotted in Fig. 2).

Definition 2 ($\mathcal{R}(\mathcal{Q})$-semi-Markov map): Let $\mathcal{Q}$ denote a partition of Ω, and let $\mathcal{R}$ denote a sub-partition of $\mathcal{Q}$. The map $S \in \Gamma(\mathcal{R})$ is $\mathcal{R}(\mathcal{Q})$-semi-Markov if the image of each interval $R \in \mathcal{R}$ under S is an interval of the partition $\mathcal{Q}$; i.e., $S(R) \in \mathcal{Q}$ for all $R \in \mathcal{R}$.

Consider an $\mathcal{R}(\mathcal{Q})$-semi-Markov map S with linear branch functions $S_{j,m} \triangleq S|_{R_j^{(m)}}$. Let $\mathcal{D}_{\mathcal{Q}}^{(\ell)} \subset \mathcal{D}$ denote the set of density functions that are defined piecewise over $\mathcal{Q}$, such that $f_t \in \mathcal{D}_{\mathcal{Q}}^{(\ell)}$ implies $f_t|_{Q_m}$ is a polynomial function with degree not exceeding $\ell \in \mathbb{N}_0$ for each $m = 1, 2, \ldots, M$. Substitution of $f_t \in \mathcal{D}_{\mathcal{Q}}^{(\ell)}$ into (7) shows that the density $f_{t+1} = \mathcal{P}_S(f_t)$ is also a member of $\mathcal{D}_{\mathcal{Q}}^{(\ell)}$. Hence, the evolution of these densities can be characterized using matrix equations. Specifically, with a PWL $\mathcal{R}(\mathcal{Q})$-semi-Markov map S and $f_t \in \mathcal{D}_{\mathcal{Q}}^{(\ell)}$ we have

$$\mathbf{f}_{t+1} = \mathbf{P}_S^{(\ell)} \mathbf{f}_t, \tag{8}$$

where $\mathbf{f}_t$ is the order-ℓ vector representation of the density function f_t and $\mathbf{P}_S^{(\ell)}$ is the order-ℓ matrix representation of the FPO $\mathcal{P}_S$. We refer to $\mathbf{P}_S^{(\ell)}$ as the order-ℓ FPM of the system with S as evolution rule. The vectors in (8) are defined as $\mathbf{f}_t \triangleq [\mathbf{f}_{t,\ell}, \mathbf{f}_{t,\ell-1}, \ldots, \mathbf{f}_{t,0}]^T$, where $\mathbf{f}_{t,\ell} \triangleq [f_{t,\ell,1}, f_{t,\ell,2}, \ldots, f_{t,\ell,M}]$ and

$$f_{t,\ell,m} = \frac{1}{\ell!} \frac{d^\ell}{dx^\ell} f_t|_{Q_m}(x)\Big|_{x=0}. \tag{9}$$

We provide expressions for the order-zero and order-one FPMs, which characterize the evolution of PWC and PWL density functions, respectively. Let S be given by

$$S(x) = \sum_{m=1}^{M} \sum_{j=1}^{c(m)} S_{j,m}(x) \chi_{R_j^{(m)}}(x). \tag{10}$$

Furthermore, let each branch function $S_{j,m}$ be given by

$$S_{j,m}(x) = v_{j,m} x + w_{j,m}. \tag{11}$$

The order-one FPM, $\mathbf{P}_S^{(1)}$, is then derived using (7) as

$$\mathbf{P}_S^{(1)} = \begin{pmatrix} \mathbf{Q}_S & \mathbf{0}_{M\times M} \\ \mathbf{R}_S & \mathbf{P}_S^{(0)} \end{pmatrix}, \tag{12}$$

where $\mathbf{Q}_S \triangleq [q_{k,m}]_{k,m=1}^M$, $\mathbf{R}_S \triangleq [r_{k,m}]_{k,m=1}^M$, and $\mathbf{0}_{M\times M}$ denotes the $M \times M$ matrix containing zeros. The elements of the submatrices $\mathbf{Q}_S$ and $\mathbf{R}_S$ are given by

$$q_{k,m} = \begin{cases} \displaystyle\sum_{j\in T(k,m)} s_{j,m} \frac{1}{v_{j,m}^2}, & \text{if } |T(k,m)| > 0 \\ 0, & \text{if } |T(k,m)| = 0, \end{cases} \tag{13}$$

and

$$r_{k,m} = \begin{cases} \displaystyle -\sum_{j\in T(k,m)} s_{j,m} \frac{w_{j,m}}{v_{j,m}^2}, & \text{if } |T(k,m)| > 0 \\ 0, & \text{if } |T(k,m)| = 0, \end{cases} \tag{14}$$

where

$$T(k,m) \triangleq \{j : S(R_j^{(m)}) = Q_k\}. \tag{15}$$

In these expressions, $s_{j,m} \triangleq \operatorname{sgn}(v_{j,m})$, where

$$\operatorname{sgn}(x) \triangleq \begin{cases} -1 & \text{if } x < 0 \\ 1 & \text{if } x \geq 0. \end{cases} \tag{16}$$

The order-zero FPM $\mathbf{P}_S^{(0)} \triangleq [p_{k,m}]_{k,m=1}^M$ has elements

$$p_{k,m} = \begin{cases} \displaystyle\sum_{j\in T(k,m)} |v_{j,m}|^{-1}, & \text{if } |T(k,m)| > 0 \\ 0, & \text{if } |T(k,m)| = 0. \end{cases} \tag{17}$$

The Folklore theorem establishes conditions for the existence and uniqueness of absolutely continuous invariant measures of systems with piecewise C^2 Markov maps as evolution rules [8]. Let $S \in \Gamma(\mathcal{R})$ denote a PWL $\mathcal{R}(\mathcal{Q})$-semi-Markov map that is aperiodic and piecewise expanding. By the Folklore theorem, S realizes a unique absolutely continuous invariant measure P_S^*, which implies that the system is ergodic. Since P_S^* is absolutely continuous, it is associated with a unique stationary density function f_S^*. This density is a fixed point of the FPO, and can be chosen as a PWC function with discontinuities only at the partition points $P(\mathcal{Q})$, such that $K^{-1} \leq f_S^* \leq K$ for some $K > 0$.

Suppose that S satisfies the conditions of the Folklore theorem. The order-zero FPM of the corresponding system is then similar to a stochastic matrix and has a unity maximal eigenvalue λ_1, referred to as the *Perron eigenvalue* [10]. This eigenvalue is a simple root of the characteristic polynomial of the matrix. It is associated with a left eigenvector (the left Perron eigenvector) that coincides with the lengths of the intervals in $\mathcal{Q}$, and a right eigenvector $\mathbf{f}_S^*$ (the right Perron eigenvector) that coincides with the PWC stationary density

f_S^*. The remaining eigenvalues of the matrix are strictly smaller than λ_1 in magnitude.

For the remainder of this section, let $S \in \Gamma(\mathcal{R})$ denote a PWL $\mathcal{R}(\mathcal{Q})$-semi-Markov map that satisfies the conditions of the Folklore theorem, and let this map be configured as the system indicated in Fig. 1. Below, we present expressions for the statistical metrics (i.e., the PDF, ACF and PSD) of the system's zero-input response.

A consequence of Birkhoff's ergodicity theorem is that time averages computed over the zero-input response are equal to their corresponding ensemble averages [47]. Using this property, expressions may be derived for the PDF f_S and ACF ϕ_S of the system's zero-input response, as defined in (3) and (5), respectively. In particular, it may be shown that the PDF f_S coincides with the unique stationary density f_S^* (i.e., the fixed point of the FPO associated with S) [46]. Hence,

$$f_S(x) = f_S^*(x) = \sum_{m=1}^{M} f_{S,m}^* \chi_{Q_m}(x), \tag{18}$$

where $\mathbf{f}_S^* \triangleq [f_{S,1}^*, f_{S,2}^*, \ldots, f_{S,M}^*]^T$ is the right Perron eigenvector of the order-zero FPM associated with S.

An expression for the ACF ϕ_S of the system's zero-input response was derived in [49]. This expression is given by

$$\phi_S(\tau) = \mathbf{g}^T \left(\mathbf{P}_S^{(1)}\right)^{|\tau|} \mathbf{h}, \tag{19}$$

where $\mathbf{h} \triangleq [(\mathbf{f}_S^*)^T, \mathbf{0}_{1\times M}]^T$ and $(\mathbf{P}_S^{(1)})^0 \triangleq \mathbf{I}$. In this expression $\mathbf{g} \triangleq [\mathbf{g}_3, \mathbf{g}_2]^T$, where the elements of $\mathbf{g}_2 \triangleq [g_{2,1}, g_{2,2}, \ldots, g_{2,M}]$ and $\mathbf{g}_3 \triangleq [g_{3,1}, g_{3,2}, \ldots, g_{3,M}]$ are given by $g_{n,m} \triangleq (q_{m+1}^n - q_m^n)/n$.

The block structure of $\mathbf{P}_S^{(1)}$ in (12) implies that the eigenvalues of this matrix comprise the eigenvalues of $\mathbf{P}_S^{(0)}$ (denoted by $\lambda_1, \lambda_2, \ldots, \lambda_M$) and the eigenvalues of $\mathbf{Q}_S$ (denoted by $\lambda_{M+1}, \lambda_{M+2}, \ldots, \lambda_{2M}$) [50]. Now, assume that $\mathbf{P}_S^{(1)}$ is diagonalizable (the general case is considered in [42]), and let $\mathbf{u}_m^T$ and $\mathbf{v}_m$ denote the left and right eigenvectors of $\mathbf{P}_S^{(1)}$ that are associated with eigenvalue λ_m. We assume each eigenvector is scaled such that $\mathbf{u}_m^H \mathbf{v}_m = 1$, where $\mathbf{u}_m^H$ is the conjugate transpose of $\mathbf{u}_m$. Equation (19) may then be simplified as

$$\phi_S(\tau) = \sum_{m=1}^{2M} c_m \lambda_m^{|\tau|}, \tag{20}$$

where

$$c_m = \mathbf{g}^T \mathbf{v}_m \mathbf{u}_m^H \mathbf{h}, \quad m = 1, 2, \ldots, 2M, \tag{21}$$

and $\lambda_m^0 \triangleq 1$ if $\lambda_m = 0$. This expression implies that the PSD of the system's zero-input response is a superposition of $2M$ spectral modes, each associated with an eigenvalue of its order-one FPM. The center frequency of mode m is equal to $\arg(\lambda_m)$, and its bandwidth is inversely proportional to $|\lambda_m|$.

The ergodicity of S implies that ϕ_S is bounded, and hence

$$\phi_S(\tau) = \sum_{\{m:|\lambda_m|=1\}} c_m \lambda_m^{|\tau|} + \underbrace{\sum_{\{m:0\le|\lambda_m|<1\}} c_m \lambda_m^{|\tau|}}_{\tilde{\phi}_S(\tau)}. \tag{22}$$

The modes in the first sum on the right-hand side of (22) coincide with spectral lines in the PSD, and constitute its impulsive component. The modes in the second sum constitute the continuous component of the PSD.

The continuous component $\tilde{\Phi}_S$ of the PSD is defined as

$$\tilde{\Phi}_S(\omega) \triangleq \tilde{\Psi}_S(z)|_{z=e^{i\omega}}, \quad \omega \in [-\pi, \pi), \tag{23}$$

where $\tilde{\Psi}_S(z)$ is the bilateral z-transform of $\tilde{\phi}_S(\tau)$ [37]. It follows that

$$\tilde{\Psi}_S(z) = \sum_{\{m:\lambda_m=0\}} c_m + \sum_{\{m:0<|\lambda_m|<1\}} \frac{c_m(1-\lambda_m^2)}{(z-\lambda_m)(z^{-1}-\lambda_m)}, \tag{24}$$

where the region of convergence is to be defined below.

Let $\tilde{\lambda}_1, \tilde{\lambda}_2, \ldots, \tilde{\lambda}_{M_P}$ denote the *unique* eigenvalues amongst $\lambda_1, \lambda_2, \ldots, \lambda_{2M}$ that satisfy $0 < |\lambda_m| < 1$. Equation (24) then yields

$$\tilde{\Psi}_S(z) = K_S H_S(z) H_S(z^{-1}), \tag{25}$$

where K_S is a scalar constant,

$$H_S(z) \triangleq \frac{\prod_{m=1}^{M_Z}(z-\eta_m)}{\prod_{m=1}^{M_P}(z-\kappa_m)}, \quad 0 \le M_Z \le M_P, \tag{26}$$

and

$$\kappa_m = \tilde{\lambda}_m, \quad m = 1, 2, \ldots, M_P. \tag{27}$$

The region of convergence of (26) is $L < |z| < L^{-1}$, where $L \triangleq \max\{0, |\tilde{\lambda}_1|, |\tilde{\lambda}_2|, \ldots, |\tilde{\lambda}_{M_P}|\}$. The numerator and denominator of (26) is defined as unity if $M_Z = 0$ or $M_P = 0$, respectively. If $\alpha \neq 0$ is a root of the numerator or denominator of $\tilde{\Psi}_S(z)$, then so is α^{-1}. Hence, the roots of its numerator and denominator appear in pairs. We define η_m such that $|\eta_m| \le 1$, $m = 1, 2, \ldots, M_Z$.

Equations (25) and (26) imply that the continuous component of the PSD is a rational function. We refer to $\kappa_1, \kappa_2, \ldots, \kappa_{M_P}$ and $\eta_1, \eta_2, \ldots, \eta_{M_Z}$ as the *poles* and *zeros* of the PSD's continuous component. Equation (27) implies that these poles are equal to the unique nonzero and nonunity (in magnitude) eigenvalues of the system's order-one FPM. As the eigenvalues $\lambda_m \in \mathbb{C} \setminus \mathbb{R}$ of a real matrix appear in complex conjugate pairs, so do the corresponding poles.

This paper addresses the design of the continuous component of the PSD belonging to the system's zero-input response, and not its impulsive component. Henceforth, for the sake of brevity, we refer to the *continuous component* of a system's PSD as *the system's PSD*, unless explicitly stated otherwise.

III. LITERATURE REVIEW

Section III-A presents a brief overview of recent advances in the nonlinear systems and control domains. A survey of existing methods for solving the inverse Frobenius-Perron system design problem is presented in section III-B.

A. ADVANCES IN NONLINEAR SYSTEMS RESEARCH

Recently, data-driven predictive control methods, where machine learning techniques are used to model the dynamical behavior of a large class of nonlinear systems, have received considerable attention in the literature (refer to the survey in [51]). Two promising control frameworks in this domain are Koopman-based model predictive control [52] and data-enabled predictive control [53], both of which are able to formulate the optimization problem in a convex form despite the nonlinearity of the underlying system. These methods have been successfully applied for process control in industries such as chemical engineering [54], [55], [56], power systems [57], [58], [59], autonomous vehicles [60], [61] and robotics [62], [63].

Networked multi-agent systems (MASs) are applied to solve complex tasks in areas such as space-based applications, smart grids, machine learning and UAV missions [64]. Recent breakthroughs have been reported on the control problem for nonlinear MASs. A novel neural network-based control scheme for the predefined-time adaptive MAS tracking control problem is proposed in [65]. The distinguishing feature of this scheme is the ability for the designer to specify the convergence time of the controlled system. Related theory was applied in [66] to develop a general consensus tracking control scheme for multi-UAV systems, where specified tracking accuracy can be achieved in a predefined time frame. The feasibility and effectiveness of the proposed control scheme was verified through its application to power network inspection missions.

B. SOLUTIONS OF THE IFPP

In the literature, the IFPP is often not formulated from the systems perspective and is instead formulated as the problem of designing a map S with prescribed statistics. Hence, terms such as ergodic, stationary density, ACF and PSD are associated with the map and not with a system configured to use the map as its evolution rule. By assuming the system indicated in Fig. 1, the theory and results reported in such works are compatible with the systems perspective of this paper. However, in the interest of simplicity, we use the map perspective to describe prior work in this section.

IFPP-I, which requires the construction of an ergodic map with a prescribed stationary density function, has been addressed extensively in the literature; refer to the recent survey article [10]. Three solution strategies have emerged for this problem. These are the topological conjugation [11], direct solution [67] and matrix solution strategies [48], [68], [69], [70], [71], [72]. Methods developed to utilize these strategies are mature and well understood; some recent examples are described in [73], [74], [75], [76], [77], and [78]. Several applications of these methods have also been reported in the literature [9], [15], [16], [17], [18], [79], and [80]. Recently, the matrix solution strategy has also been utilized to reconstruct a map from sequences of density functions generated by it [13], [14], [81], [82], [83].

This paper addresses IFPP-II, which requires the map to possess a prescribed stationary density function as well as a prescribed ACF or PSD. IFPP-II has not been addressed as comprehensively as IFPP-I in the literature. The most relevant methods aimed at solving IFPP-II are reviewed below.

Baranovsky and Daems [12] investigated the problem of constructing one-dimensional chaotic maps with a prescribed stationary density and ACF. A class of complete PWL Markov maps that possess the uniform stationary density was defined. It was shown that these maps possess an ACF that corresponds with a single spectral mode. An analytical method was proposed for constructing a map, having a prescribed spectral mode, from this class. Whereas a topological conjugate of this map may be constructed to possess the exact prescribed stationary density, in general, the conjugate map's ACF does not equal that of the original map. However, these ACFs were shown to be approximately equal if the Markov partition $\mathcal{Q}$ of the original map is selected such that the conjugating transformation can be closely approximated by a PWL function defined over $\mathcal{Q}$. The proposed method selects the Markov partition in this manner and thus constructs a topological conjugate having the prescribed stationary density and an ACF approximating a prescribed mode. Whereas the PSDs realizable using the method are limited to a single mode, a more general class of non-Markov maps that possess a PSD with multiple modes was investigated. However, the design of these non-Markov maps was not addressed.

Diakonos et al. [38] proposed a groundbreaking numerical method for generating unimodal maps that possess a prescribed stationary density and (in part) a prescribed ACF. The method relates the branch pre-images of any complete unimodal map that possesses the prescribed stationary density to each other using a parametric inter-branch correspondence function. The real-valued parameters of this function serve as an index into a set of unimodal maps that share the prescribed stationary density. An objective function that quantifies the deviation of the first n values of the candidate map's ACF from the prescribed function was defined. A numerical search for a candidate map that minimizes this objective function is performed by varying the parameters of the inter-branch correspondence function. Whereas examples that demonstrate the method's potential were presented, it may fail to converge to a map having an ACF with the prescribed values due to the high dimensionality of the search space. Also, the class of PSDs realizable by the method is unknown, and its computational complexity increases exponentially with n.

The methods in [39], [40], and [41] aim to solve IFPP-II by constructing semi-Markov maps. This map choice is motivated by two observations. First, the PWL semi-Markov maps possess a rational PSD which, if fully specifiable, can be selected to approximate any continuous PSD to the desired degree of accuracy. Second, the explicit relationship between the relevant statistical metrics of a PWL semi-Markov

map and its order-one FPM permits the use of *analytical* methods that are immune to numerical impairments and non-convergence.

The methods in [39], [40], and [41] generalize the matrix solution of IFPP-I first proposed in [48]. Each method constructs a stochastic matrix with prescribed characteristics, and which qualifies as the order-zero FPM of a PWL semi-Markov map. A particular map from this class is then constructed such that its order-zero FPM equals the stochastic matrix. We observe that multiple distinct maps from this class may be constructed to possess a prescribed stochastic matrix as order-zero FPM.

The method proposed in [40] constructs a semi-Markov map with stationary density that approximates a prescribed density function and a PSD with an arbitrary number of poles, such that non-repeating real values may be prescribed for a *proper* subset of the poles. It uses the observation that the unique nonzero and nonunity (in magnitude) eigenvalues of the map's order-zero FPM appear as poles in its PSD. The method uses recursive Markov state disaggregation [84] to construct a doubly stochastic matrix (i.e., a nonnegative matrix with rows and columns that sum to unity) of arbitrary dimensionality and with a real eigenspectrum selected to equal the prescribed poles. A PWL semi-Markov map that possesses the uniform stationary density and a single branch for each nonzero entry of this matrix (i.e., its order-zero FPM) is then constructed. A topological conjugate of this map, itself a PWL semi-Markov map, is constructed in the final step. The PWC stationary density of the conjugate map is selected to approximate the prescribed stationary density. It is shown that the eigenspectra of the original map's and conjugate map's order-zero FPMs are equal. Hence, a proper subset of the poles belonging to the conjugate map's PSD (i.e., those that correspond to the order-zero FPM eigenspectrum) may be prescribed. The method permits prescription of real-valued poles only, limiting these power spectrum modes to center frequencies of zero and π radians per second. Furthermore, neither the zeros, nor the remaining poles of the PSD (corresponding to the order-one FPM's remaining eigenvalues) can be prescribed.

Expressions for 3×3 doubly stochastic matrices with a prescribable *complex-valued* eigenspectrum were derived in [41]. A method was proposed that constructs a doubly stochastic matrix using these expressions and a PWL semi-Markov map with order-zero FPM that is equal to the matrix. These maps are constructed in the same manner as [40] and possess a stationary density that is uniform over the unit interval. The method permits selection of the same proper subset of PSD poles as the method of [40], but these poles may now assume complex values. However, the zeros and remaining poles cannot be prescribed, and the maps are limited to a maximum of five poles only, due to the dimensions of the order-one FPM (here, the order-one FPM has six eigenvalues, of which one eigenvalue is necessarily equal to unity).

The methods in [40] and [41] permit the selection of the map's order-zero FPM, but not its order-one FPM. Hence, the PSD poles that coincide with the eigenvalues of the top-left submatrix $\mathbf{Q}_S$ of the order-one FPM in (12) cannot be directly specified using these methods. A different approach proposed in [39] permits the construction of members from a subset of the semi-Markov maps that are distinct from those considered in [40] and [41]. The structure of these *PWL hat maps prevents* the eigenvalues belonging to submatrix $\mathbf{Q}_S$ of the order-one FPM from appearing as poles in the map's PSD. Equations (24) to (27) imply that the poles of the PSD are restricted to the unique nonzero and nonunity (in magnitude) eigenvalues of the order-zero FPM and submatrix $\mathbf{Q}_S$. In Proposition 1 we formally prove that submatrix $\mathbf{Q}_S$ of the order-one FPM belonging to any PWL hat map is the *zero matrix*, which has eigenvalues only equal to zero. Thus, the spectral modes associated with the eigenvalues of $\mathbf{Q}_S$ appear in the PSD with uniform magnitude over frequency.

The method proposed in [39] constructs a semi-Markov map with nonlinear branches and prescribed stationary density such that its PWL approximation, which is itself a PWL hat map, possesses an order-zero FPM equal to a prescribed stochastic matrix. A numerical algorithm is used to construct a stochastic matrix with a specified eigenspectrum, thereby prescribing all the poles of the PWL hat map's PSD. Although numerical examples suggest that the PSDs of the map with nonlinear branches and the PWL hat map are approximately equal, the relationship is not established analytically. In certain cases, it was also observed that the method fails to converge to a map with the prescribed statistics.

We conclude this section by considering the possible extension of a particular matrix solution of IFPP-I [69], [70], [71], [72] to address IFPP-II. The method developed in these works constructs semi-Markov maps with an $M \times M$ order-zero FPM having a particular structure, which is completely specified by a collection of $2M$ real-valued parameters. Of particular interest is the fact that the parameters of this matrix may be selected to specify upper and lower bounds in between which the individual eigenvalues of the matrix must fall. Considering the relationship between the eigenvalues of the order-zero FPM and the map's spectral modes, this method may afford some freedom to select the spectral characteristics of the map, but the authors of these works did not address IFPP-II. However, we observe that the parameters of the relevant matrix cannot be selected to guarantee tight bounds for *all* of its eigenvalues. Furthermore, all eigenvalues of the matrix are necessarily positive, which implies that a solution to IFPP-II that utilizes this matrix can only allow for the prescription of PSD poles that lie on the positive real axis in the complex plane. Stated differently, such a method would only be able to realize spectral modes with center frequencies of zero radians per sample. Hence, the use of the matrix proposed in [69], [70], [71], and [72] to solve IFPP-II necessarily imposes strong restrictions on the realizable PSDs.

IV. NOVEL METHOD FOR SYSTEM DESIGN

The novel method proposed in this paper designs a system with a zero-input response that has a PWC PDF. This PDF is selected to approximate an arbitrary PDF prescribed for the system's zero-input response. The method simultaneously realizes a rational PSD with an arbitrary number of poles for the system response, and permits the prescription of non-repeating complex values for *all* of these poles.

The novel method uses a recent analytical technique [43] to construct a stochastic matrix $\mathbf{P}$ with complex-valued eigenspectrum selected to equal the prescribed non-repeating poles (step one). Similarly to the method of [40], a PWL hat map S is then constructed such that a system configured to use the map as its evolution rule has an order-zero FPM equal to the matrix $\mathbf{P}$ (step two). As described in section III, this permits prescription of all the poles through the selection of the eigenspectrum of $\mathbf{P}$. A topological conjugate $\tilde{S}$ of the map S, which is a PWL hat map that realizes the same poles as S, is then constructed (step three). The conjugate map is designed such that the system configured to use this map, as indicated in Fig. 1, generates a zero-input response with a PWC PDF that approximates the prescribed response PDF. Each step of the novel method is described below.

A. CONSTRUCTION OF A STOCHASTIC MATRIX

Let $\kappa_1, \kappa_2, \ldots, \kappa_{M_P}$ denote the prescribed non-repeating poles. We first construct an $M \times M$ stochastic matrix, where $M \triangleq M_P + 1$. The eigenvalues of this matrix are selected as

$$\lambda_1 = 1 \tag{28}$$

and

$$\lambda_m = \kappa_{m-1}, \qquad m = 2, \ldots, M_P + 1. \tag{29}$$

The problem of constructing a stochastic matrix with a prescribed eigenspectrum is referred to as the stochastic inverse eigenvalue problem (StIEP) [85]. Iterative methods that aim to solve the StIEP numerically are prominent in the literature (recent examples appear in [86], [87]). These methods attempt to numerically minimize a cost function, thereby converging to a matrix with the prescribed eigenspectrum. However, the StIEP is an ill-posed problem, and the performance of such methods depends strongly on the distribution of the prescribed eigenvalues [87]. The work presented here considers an analytical solution instead.

In this paper we use a recently proposed analytical solution to the StIEP [43] that directly constructs matrices with prescribed complex-valued eigenspectra. This solution generalizes an earlier solution [84] which is limited to constructing matrices with real-valued eigenspectra. Both solutions use Markov state disaggregation to construct a Markov chain with a stochastic transition matrix possessing the required eigenspectrum. Unlike solutions that rely on numerical methods, these analytical solutions construct the matrix after a finite and predetermined number of iterations, and without numerical approximation. We describe the solution steps, but do not elaborate on the connection with Markov chains.

The StIEP solution of [43] uses the single-element matrix $\mathbf{P} = [1]$, which possesses the unity eigenvalue, as a starting point. This matrix is repeatedly enlarged over a predetermined number of rounds, thereby producing a stochastic matrix with the prescribed eigenspectrum. Matrix enlargement is achieved by applying a *disaggregation technique* during each round. This involves the selection and replacement of a positive diagonal element of $\mathbf{P}$ with a particular $K \times K$ matrix (where $K > 1$), and the systematic definition of the new elements of $\mathbf{P}$ appearing in the same rows and columns as the elements of the inserted matrix. We select the inserted matrix and the new elements of $\mathbf{P}$ to insert one or more prescribed eigenvalues into the eigenspectrum of $\mathbf{P}$, while simultaneously leaving its existing eigenvalues unaltered and ensuring that it remains stochastic.

We distinguish between two disaggregation techniques, referred to as the *original* and *novel* techniques (these were first proposed in [43] and [84], respectively). Whereas the original technique permits the insertion of a single real eigenvalue into the eigenspectrum of $\mathbf{P}$, the novel technique permits the insertion of a complex conjugate pair of eigenvalues from the set $\mathbb{C} \setminus \mathbb{R}$ (i.e., the *strictly complex* eigenvalues). These techniques are used in tandem by the solution of [43] to insert the prescribed eigenvalues into the eigenspectrum of the single-element matrix over the number of rounds required, thereby producing a stochastic matrix that possesses the prescribed complex-valued eigenspectrum.[5]

For the purpose of defining the original and novel disaggregation techniques, we express the $N \times N$ matrix $\mathbf{P}$ at the start of a particular round as

$$\mathbf{P} = \left(\begin{array}{c|c|c} \mathbf{P}_{1,1} & \mathbf{v}_{1,k} & \mathbf{P}_{1,2} \\ \hline \mathbf{w}_{k,1}^T & p_{k,k} & \mathbf{w}_{k,2}^T \\ \hline \mathbf{P}_{2,1} & \mathbf{v}_{2,k} & \mathbf{P}_{2,2} \end{array}\right). \tag{30}$$

We apply the disaggregation techniques in a manner to ensure that the elements of $\mathbf{P}$ remain positive. The Perron-Frobenius theorem [88] then implies that $\mathbf{P}$ possesses a unique maximal eigenvalue (i.e., the Perron eigenvalue) equal to unity, and that its corresponding right Perron eigenvector $\boldsymbol{\pi} = [\pi_1, \pi_2, \ldots, \pi_N]^T$ has strictly positive elements.

Below, we define the original and novel disaggregation techniques, and the algorithm used to solve the StIEP.

1) ORIGINAL DISAGGREGATION TECHNIQUE

Suppose that $\mathbf{P}$ in (30) is to be enlarged using the original disaggregation technique of [84], and let its diagonal element $p_{k,k}$ be selected for replacement. The matrix is enlarged by one row and one column to insert a single real eigenvalue λ into its eigenspectrum, thereby obtaining $\mathbf{P}'$. The process of applying the original technique in this manner is expressed as

[5] Any stochastic matrix has at least one unity eigenvalue. Therefore, using the single-element matrix $\mathbf{P} = [1]$ as the starting point does not lead to an incompatible eigenspectrum. We also note that the strictly complex eigenvalues of any real matrix necessarily appear in complex conjugate pairs.

$\mathbf{P}' = \mathcal{T}(\mathbf{P}, \lambda, \alpha, k)$, where $\mathcal{T} : \mathbb{P}_N \to \mathbb{P}_{N+1}$ and $\mathbb{P}_N$ is the set of all $N \times N$ stochastic matrices. Here, α denotes a real parameter that is selected in order to choose certain elements of the right Perron eigenvector belonging to $\mathbf{P}'$. Matrix $\mathbf{P}'$ is defined as

$$\mathbf{P}' \triangleq \left(\begin{array}{c|cc|c} \mathbf{P}_{1,1} & \mathbf{v}_{1,k} & \mathbf{v}_{1,k} & \mathbf{P}_{1,2} \\ \hline \alpha\mathbf{w}_{k,1}^T & \multicolumn{2}{c|}{\multirow{2}{*}{$\mathbf{T}$}} & \alpha\mathbf{w}_{k,2}^T \\ (1-\alpha)\mathbf{w}_{k,1}^T & & & (1-\alpha)\mathbf{w}_{k,2}^T \\ \hline \mathbf{P}_{2,1} & \mathbf{v}_{2,k} & \mathbf{v}_{2,k} & \mathbf{P}_{2,2} \end{array}\right), \tag{31}$$

where $\mathbf{T} \triangleq T(p_{k,k}, \lambda, \alpha)$ is a 2×2 matrix. The operator $T(p_{k,k}, \lambda, \alpha)$ is defined as

$$T(p_{k,k}, \lambda, \alpha) \triangleq \frac{p_{k,k}}{h_{\max}} \begin{pmatrix} \alpha & \alpha - h_{\min} \\ h_{\max} - \alpha & 1 - \alpha \end{pmatrix}, \tag{32}$$

where $h_{\max} \triangleq p_{k,k}/(p_{k,k} + \lambda)$ and $h_{\min} \triangleq \lambda/(p_{k,k} + \lambda)$.

To produce a positive stochastic matrix $\mathbf{P}'$, the parameters λ and α must be selected to satisfy

$$|\lambda| < p_{k,k} \tag{33}$$

and

$$\max\{h_{\min}, 0\} < \alpha < \min\{h_{\max}, 1\}. \tag{34}$$

The following theorems outline relevant properties of the original disaggregation technique. We assume in each case that element $p_{k,k}$ of $\mathbf{P}$ is replaced during disaggregation.

Theorem 1: Matrix $\mathbf{P}'$ inherits the eigenvalues of $\mathbf{P}$, and gains the additional real eigenvalue λ.

Proof: Refer to [84, Th. 3.1]. □

Theorem 2: Matrix $\mathbf{P}'$ possesses the right Perron eigenvector $\boldsymbol{\pi}' = [\pi'_1, \pi'_2, \ldots, \pi'_{N+1}]^T$ with elements that satisfy

$$\pi'_i = \begin{cases} \pi_i, & \text{if } i < k \\ \beta\pi_k & \text{if } i = k \\ (1-\beta)\pi_k, & \text{if } i = k+1 \\ \pi_{i-1}, & \text{if } i > k+1, \end{cases} \tag{35}$$

where

$$\beta \triangleq \frac{\alpha(1+\lambda) - \lambda}{1 - \lambda}. \tag{36}$$

Proof: Refer to [84, Th. 2.6]. □

Theorem 2 implies that original disaggregation replaces element π_k of the right Perron eigenvector $\boldsymbol{\pi}$ with two positive elements that sum to π_k, thereby producing the new right Perron eigenvector $\boldsymbol{\pi}'$ belonging to $\mathbf{P}'$. The values of these elements may be selected by specifying an appropriate value for α, thereby choosing β according to (36).

2) NOVEL DISAGGREGATION TECHNIQUE

Suppose that $\mathbf{P}$ in (30) is to be enlarged using the novel disaggregation technique of [43], and let its diagonal element $p_{k,k}$ be selected for replacement. The matrix is enlarged by two rows and two columns to insert a conjugate pair of strictly complex eigenvalues $\lambda = re^{i\theta}$ and $\lambda^* = re^{-i\theta}$ into its eigenspectrum, thereby obtaining $\mathbf{P}'$. We express the process of applying the novel technique in this manner as $\mathbf{P}' = \mathcal{U}(\mathbf{P}, r, \theta, k)$, where $\mathcal{U} : \mathbb{P}_N \to \mathbb{P}_{N+2}$. Matrix $\mathbf{P}'$ is defined as

$$\left(\begin{array}{c|ccc|c} \mathbf{P}_{1,1} & \mathbf{v}_{1,k} & \mathbf{v}_{1,k} & \mathbf{v}_{1,k} & \mathbf{P}_{1,2} \\ \hline \mathbf{w}_{k,1}^T/3 & \multicolumn{3}{c|}{\multirow{3}{*}{$\mathbf{U}$}} & \mathbf{w}_{k,2}^T/3 \\ \mathbf{w}_{k,1}^T/3 & & & & \mathbf{w}_{k,2}^T/3 \\ \mathbf{w}_{k,1}^T/3 & & & & \mathbf{w}_{k,2}^T/3 \\ \hline \mathbf{P}_{2,1} & \mathbf{v}_{2,k} & \mathbf{v}_{2,k} & \mathbf{v}_{2,k} & \mathbf{P}_{2,2} \end{array}\right), \tag{37}$$

where $\mathbf{U} \triangleq U(p_{k,k}, r, \theta)$ is a 3×3 matrix. The operator $U(p_{k,k}, r, \theta)$ is defined as

$$U(p_{k,k}, r, \theta) \triangleq \begin{pmatrix} \nu_1 & \nu_2 & \nu_3 \\ \nu_3 & \nu_1 & \nu_2 \\ \nu_2 & \nu_3 & \nu_1 \end{pmatrix}, \tag{38}$$

where

$$\nu_1 \triangleq \nu_1(p_{k,k}, r, \theta) = \frac{p_{k,k}}{3} + \frac{2r}{3}\cos\theta, \tag{39}$$

$$\nu_2 \triangleq \nu_2(p_{k,k}, r, \theta) = \frac{p_{k,k}}{3} - \frac{r}{3}(\cos\theta - \sqrt{3}\sin\theta), \tag{40}$$

and

$$\nu_3 \triangleq \nu_3(p_{k,k}, r, \theta) = \frac{p_{k,k}}{3} - \frac{r}{3}(\cos\theta + \sqrt{3}\sin\theta). \tag{41}$$

The region of permissible values for λ is defined by

$$\mathrm{Re}(\lambda) > -\frac{p_{k,k}}{2}, \tag{42}$$

$$\frac{1}{\sqrt{3}}(\mathrm{Re}(\lambda) - p_{k,k}) < \mathrm{Im}(\lambda) < -\frac{1}{\sqrt{3}}(\mathrm{Re}(\lambda) - p_{k,k}), \tag{43}$$

and

$$\theta \neq k\pi, \quad k \in \mathbb{Z}. \tag{44}$$

This region coincides with the interior of the shaded triangle in the complex plane of Fig. 3, with the real line excluded.

The following theorems outline relevant properties of the novel disaggregation technique. We assume in each case that element $p_{k,k}$ of $\mathbf{P}$ is replaced during disaggregation.

Theorem 3: Matrix $\mathbf{P}'$ inherits the eigenvalues of $\mathbf{P}$, and gains the complex conjugate pair of eigenvalues λ and λ^*.

Proof: Refer to [43, Th. 3.3]. □

Theorem 4: Matrix $\mathbf{P}'$ possesses the right Perron eigenvector $\boldsymbol{\pi}' = [\pi'_1, \pi'_2, \ldots, \pi'_{N+2}]^T$ with elements that satisfy

$$\pi'_i = \begin{cases} \pi_i, & \text{if } i < k \\ \pi_k/3, & \text{if } i = k, k+1, k+2 \\ \pi_{i-2}, & \text{if } i > k+2. \end{cases} \tag{45}$$

Proof: Refer to [43, Th. 3.4]. □

Theorem 4 reveals that novel disaggregation replaces element π_k of the right Perron eigenvector $\boldsymbol{\pi}$ with three positive and equal elements, thereby producing the new right Perron eigenvector $\boldsymbol{\pi}'$ of $\mathbf{P}'$. In contrast to the original disaggregation technique, novel disaggregation affords no freedom to select the new elements of the right Perron eigenvector.

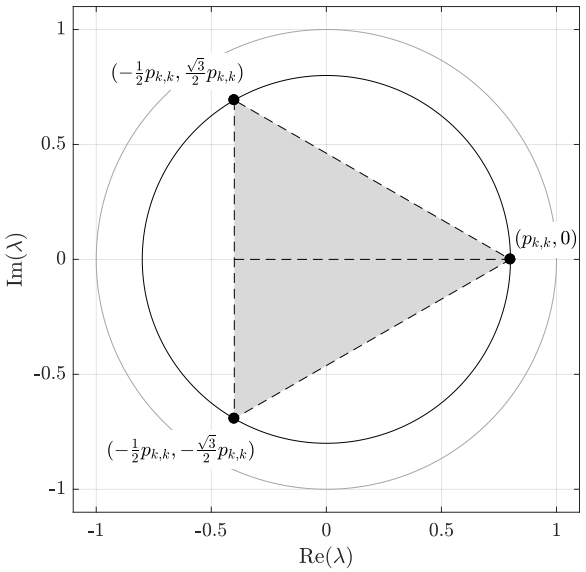


FIGURE 3. Complex plane with shaded region representing the permissible values for eigenvalue $\lambda = re^{i\theta}$ when applying the novel disaggregation technique. The parameter $p_{k,k} = 0.8$ was used in the figure. Reproduced with permission from [43].

3) ALGORITHM FOR SOLVING THE STIEP

There exist multiple degrees of freedom when applying the disaggregation techniques to solve the StIEP. These include the order in which eigenvalues are inserted into the eigenspectrum, as well as the matrix element to replace and (in the case of original disaggregation) the parameter α in each round of matrix enlargement. Choices made during earlier rounds of matrix enlargement may lead to a prescribed eigenvalue becoming inadmissible for insertion into the eigenspectrum during later rounds, even though a stochastic matrix with the prescribed eigenspectrum exists.

An algorithm for solving the StIEP that aims to prevent the situation described above was proposed in [43]. This algorithm inserts the prescribed eigenvalues into the eigenspectrum in decreasing order of their modulus. Also, the largest element of the matrix diagonal is replaced during each round of enlargement. No rule for selecting parameter α is specified, but we observe that the selection of $\alpha = 1/2$ is always permissible, irrespective of the eigenvalue selected for insertion in the round of interest. This algorithm is used by the proposed method for system design.

B. CONSTRUCTION OF A PWL HAT MAP

We construct a PWL hat map S and configure a recursive system to use this map as its evolution rule, as indicated in Fig. 1. This hat map is designed such that the system possesses an order-zero FPM equal to the matrix $\mathbf{P}$ constructed in step one. The positivity of $\mathbf{P}$ implies that S satisfies the conditions of the Folklore theorem. Hence, the system is ergodic.

Informally, a PWL hat map S is a semi-Markov map where each consecutive pair of neighboring branches is shaped like a hat; an example is plotted in Fig. 4(a). Each pair's left and right branches share the same image under S, and possess a positive and negative slope of equal magnitude. We proceed by formally defining the class of PWL hat maps in a constructive fashion. That is, we construct a PWL hat map S that is $\mathcal{R}(\mathcal{Q})$-semi-Markov and which realizes an order-zero FPM equal to a prescribed $M \times M$ stochastic matrix $\mathbf{P}$ (that is positive). This is accomplished by (i) specifying the map's Markov partition $\mathcal{Q}$, (ii) specifying the sub-partition $\mathcal{R}$ of $\mathcal{Q}$ and selecting the image of each sub-partition interval, and (iii) specifying the monotonicity of each map branch.

Let $\mathbf{u}^T = [u_1, u_2, \ldots, u_M]$ denote the left Perron eigenvector of $\mathbf{P}$, and let it be normalized with elements that sum to unity (the Perron-Frobenius theorem implies that these elements are strictly positive). Map S possesses a Markov partition with interval lengths equal to the elements of $\mathbf{u}$ if the system's order-zero FPM equals $\mathbf{P}$. Thus, we select $\mathcal{Q} = \{Q_1, \ldots, Q_M\}$, where

$$Q_m = \left(\sum_{\ell=1}^{m-1} u_\ell, \sum_{\ell=1}^{m} u_\ell \right). \tag{46}$$

Next, we construct the sub-partition $\mathcal{R}$ of $\mathcal{Q}$ and select the images of its intervals under S. The sub-partition is constructed by specifying the partition $\mathcal{R}^{(m)}$ of each interval Q_m. As implied by (17), if element $p_{k,m}$ of any order-zero FPM associated with an $\mathcal{R}(\mathcal{Q})$-semi-Markov map is greater than zero, the map must possess at least one branch with domain equal to an interval of $\mathcal{R}^{(m)}$ and image equal to Q_k. All elements of $\mathbf{P}$ are greater than zero. Hence, each interval Q_m of $\mathcal{Q}$ must have a pre-image in $\mathcal{R}^{(m)}$ under S. We reserve *two* intervals in $\mathcal{R}^{(m)}$ for each element in column m of $\mathbf{P}$, such that $\mathcal{R}^{(m)} = \{R_1^{(m)}, R_2^{(m)}, \ldots, R_{2M}^{(m)}\}$. We specify that S maps the intervals of $\mathcal{R}^{(m)}$ to the intervals of $\mathcal{Q}$ as

$$R_{2k-1}^{(m)}, R_{2k}^{(m)} \overset{S}{\mapsto} Q_k, \qquad k = 1, 2, \ldots, M. \tag{47}$$

Equation (17) implies that the partition intervals must satisfy

$$\mu(R_{2k-1}^{(m)}) + \mu(R_{2k}^{(m)}) = p_{k,m}\mu(Q_k) \tag{48}$$

if the order-zero FPM of the system is to equal $\mathbf{P}$. We specify the intervals $R_{2k-1}^{(m)}$ and $R_{2k}^{(m)}$ to be of equal length; i.e.,

$$\mu(R_{2k-1}^{(m)}) = \mu(R_{2k}^{(m)}) = p_{k,m}\mu(Q_k)/2. \tag{49}$$

This implies that the intervals of $\mathcal{R}$ are selected as

$$R_j^{(m)} = \left(q_m + \sum_{\ell=1}^{j-1} \mu(R_\ell^{(m)}), q_m + \sum_{\ell=1}^{j} \mu(R_\ell^{(m)}) \right), \tag{50}$$

where $m = 1, 2, \ldots, M$ and $j = 1, 2, \ldots, 2M$.

The branches defined over $R_{2k-1}^{(m)}$ and $R_{2k}^{(m)}$ are specified to be linear and to possess a positive and a negative slope, respectively. The branch functions of S are thus given by

$$S_{2k-1,m}(x) \triangleq S|_{R_{2k-1}^{(m)}}(x) = \frac{2}{p_{k,m}}(x - r_{2k-1}^{(m)}) + q_k \tag{51}$$

and

$$S_{2k,m}(x) \triangleq S|_{R_{2k}^{(m)}}(x) = -\frac{2}{p_{k,m}}(x - r_{2k+1}^{(m)}) + q_k, \tag{52}$$

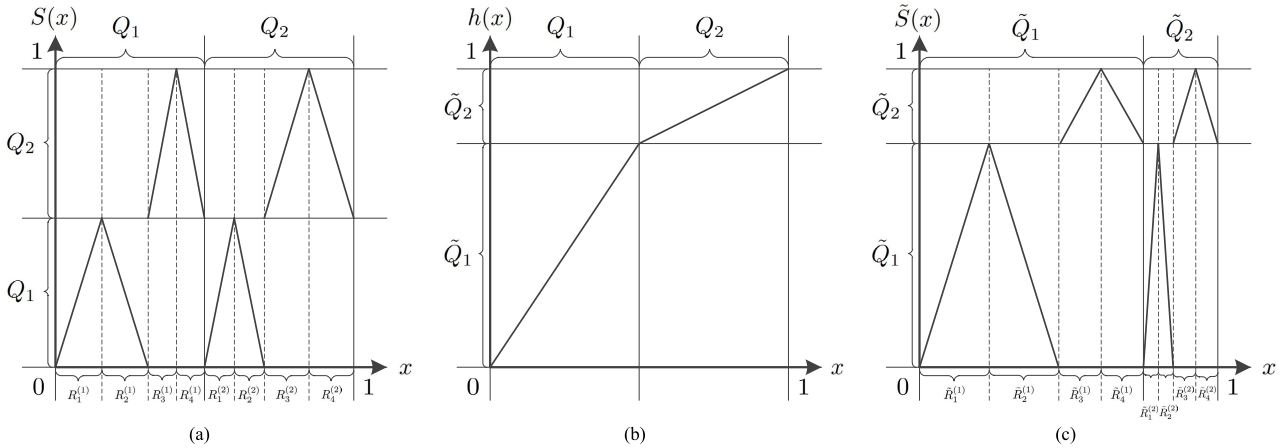


FIGURE 4. Plots of (a) a PWL hat map S, (b) a conjugating transform h, and (c) the corresponding topological conjugate $\tilde{S} = h \circ S \circ h^{-1}$ of the map S.

where $k, m = 1, 2, \ldots M$, $r_{2k-1}^{(m)} \triangleq \inf(R_{2k-1}^{(m)})$ and $r_{2k+1}^{(m)} \triangleq \sup(R_{2k}^{(m)})$. These expressions uniquely define a PWL hat map that realizes a prescribed order-zero FPM $\mathbf{P}_S^{(0)} = \mathbf{P}$.

The following propositions outline two properties of the PWL hat maps that are relevant to the problem of constructing systems with prescribed PSD poles.

Proposition 1: The top-left submatrix $\mathbf{Q}_S$ of the order-one FPM realized by any PWL hat map S is the zero matrix.

Proof: Equation (47) implies that any hat map associated with a positive order-zero FPM satisfies

$$T(k, m) = \{j : S(R_j^{(m)}) = Q_k\} = \{2k - 1, 2k\}. \tag{53}$$

Equation (13) then implies that each element $q_{k,m}$ of $\mathbf{Q}$ is given by $q_{k,m} = s_{2k-1,m}/v_{2k-1,m}^2 + s_{2k,m}/v_{2k,m}^2$, where $v_{\cdot,m}$ is the slope of $S_{\cdot,m}$ and $s_{\cdot,m} \triangleq \operatorname{sgn}(v_{\cdot,m})$. But (51) and (52) imply that $v_{2k-1,m}^2 = 4/p_{2k-1,m}^2 = v_{2k,m}^2$ and that $s_{2k-1,m} = -s_{2k,m}$. Hence, each $q_{k,m} = 0$. □

Proposition 2: Consider any PWL hat map S that realizes a system with a $2M \times 2M$ order-one FPM. The eigenspectrum of the system's order-one FPM comprises the eigenspectrum of its order-zero FPM and M zero eigenvalues.

Proof: Equation (12) shows that the order-one FPM of the system has a block lower triangular structure. The eigenspectrum of a block triangular matrix equals the eigenspectra of its diagonal blocks [50]. Since the order-one FPM's bottom-right submatrix is the order-zero FPM, and its top-left submatrix $\mathbf{Q}_S$ is the zero matrix (Proposition 1), which possesses M zero eigenvalues, the proposition follows. □

Equations (24) to (27) imply that a system configured to use a semi-Markov map as evolution rule generates a zero-input response with PSD poles that coincide with the unique nonzero and nonunity (in magnitude) eigenvalues of the system's order-one FPM. In the case of a system configured to use a hat map, Proposition 2 then implies that the PSD poles coincide with the unique nonzero and nonunity (in magnitude) eigenvalues of the system's *order-zero* FPM only. As the eigenspectrum of the order-zero FPM is prescribed during the construction of the stochastic matrix in step one (refer to section IV-A), *all* poles of the PSD may be prescribed using the novel method. This is made possible by the particular structure of the hat map.

Let S denote a PWL hat map that is $\mathcal{R}(\mathcal{Q})$-semi-Markov. If the system configured to use S as evolution rule is ergodic, the PDF of its zero-input response is PWC over the intervals of $\mathcal{Q}$. This density coincides with the right Perron eigenvector of the system's order-zero FPM. As the proposed method for constructing the stochastic matrix (as presented in section IV-A) does not permit arbitrary selection of the right Perron eigenvector, the PDF belonging to the response of the system constructed in the two steps presented thus far cannot be prescribed. However, we may construct a topological conjugate $\tilde{S}$ of the map S such that it realizes a system response with a PWC PDF that approximates a prescribed density. This final step of the novel method is described in the next subsection.

C. TOPOLOGICAL CONJUGATION

Let S denote a PWL and $\mathcal{R}(\mathcal{Q})$-semi-Markov hat map constructed using the preceding steps. A topological conjugate

$$\tilde{S} \triangleq h \circ S \circ h^{-1} \tag{54}$$

of S is constructed in the final step, which implies that the system configured to use $\tilde{S}$ as evolution rule is also ergodic [10]. A continuous and increasing conjugating transform h that linearly expands or compresses each interval of $\mathcal{Q}$ is specified (refer to Fig. 4(b) for an example of this transform). The conjugating transform h ensures that $\tilde{S}$ is a PWL hat map with a specified Markov partition $\tilde{\mathcal{Q}}$. This Markov partition has the same number of intervals as $\mathcal{Q}$ and is selected such that the zero-input response of a system configured to use $\tilde{S}$ as evolution rule has a PWC PDF that approximates a prescribed response PDF f_P^*.

We first define the conjugating transform h and then describe how $\tilde{\mathcal{Q}}$ is selected. Let $\mathcal{Q} \triangleq \{Q_1, Q_2, \ldots, Q_M\}$ and $\tilde{\mathcal{Q}} \triangleq \{\tilde{Q}_1, \tilde{Q}_2, \ldots, \tilde{Q}_M\}$. The transform h is defined as

$$h(x) \triangleq \sum_{m=1}^{M} [\Delta_m(x - q_m) + \tilde{q}_m]\chi_{Q_m}(x), \tag{55}$$

where $Q_m \triangleq (q_m, q_{m+1})$, $\tilde{Q}_m \triangleq (\tilde{q}_m, \tilde{q}_{m+1})$, and

$$\Delta_m \triangleq (\tilde{q}_{m+1} - \tilde{q}_m)/(q_{m+1} - q_m). \tag{56}$$

As h linearly maps each interval of $\mathcal{Q}$ to its counterpart in $\tilde{\mathcal{Q}}$, and its inverse h^{-1} linearly maps the intervals of $\tilde{\mathcal{Q}}$ to $\mathcal{Q}$, the conjugate map $\tilde{S} \triangleq h \circ S \circ h^{-1}$ is a PWL hat map with Markov partition equal to $\tilde{\mathcal{Q}}$. The conjugate $\tilde{S}$ of the map S in Fig 4(a) is plotted in Fig. 4(c) (the conjugating transform in Fig. 4(b) was used).

Let $\mathbf{P}^{(0)}_{\tilde{S}}$ denote the order-zero FPM associated with $\tilde{S}$. This matrix is similar to the order-zero FPM associated with S [10]; i.e.,

$$\mathbf{P}^{(0)}_{\tilde{S}} = \mathbf{\Delta}^{-1}\mathbf{P}^{(0)}_{S}\mathbf{\Delta}, \tag{57}$$

where $\mathbf{\Delta} \triangleq \text{diag}(\Delta_1, \Delta_2, \ldots, \Delta_M)$. This implies that the right Perron eigenvectors $\mathbf{f}^*_{\tilde{S}}$ and $\mathbf{f}^*_{S}$ of the order-zero FPMs realized by $\tilde{S}$ and S satisfy

$$\mathbf{f}^*_{\tilde{S}} = \mathbf{\Delta}^{-1}\mathbf{f}^*_{S}. \tag{58}$$

Recall that $\mathbf{f}^*_{\tilde{S}}$ coincides with the stationary density $f^*_{\tilde{S}}$ realized by $\tilde{S}$. This density is PWC over $\tilde{\mathcal{Q}}$. Equation (58) thus implies that the conjugating transform's expansion or compression of each Q_m (the right-hand side) lowers or elevates the stationary density f^*_S of S over that interval, thereby realizing the density $f^*_{\tilde{S}}$ over interval $\tilde{Q}_m$ (the left-hand side). As the scaling of the interval length and density level is proportional, the area under $f^*_{\tilde{S}}|_{\tilde{Q}_m}$ equals the area under $f^*_S|_{Q_m}$. This implies that the (cumulative) distribution functions $F^*_{\tilde{S}}$ and F^*_S, associated with the densities $f^*_{\tilde{S}}$ and f^*_S, are equal when evaluated at the corresponding partition points of $\tilde{\mathcal{Q}}$ and $\mathcal{Q}$; i.e.,

$$F^*_{\tilde{S}}(\tilde{q}_m) = F^*_S(q_m), \qquad m = 1, 2, \ldots, M+1, \tag{59}$$

where

$$F^*_S(q_m) = \sum_{\ell=1}^{m-1}(q_{\ell+1} - q_\ell)f^*_S|_{Q_\ell} \tag{60}$$

is known after the map S has been constructed using the second step of the novel method (section IV-B).

We select $\tilde{\mathcal{Q}}$ such that the distribution function $F^*_{\tilde{S}}$ equals the distribution function F^*_P associated with the prescribed stationary density f^*_P at each partition point $\tilde{q}_m$; i.e., $F^*_{\tilde{S}}(\tilde{q}_m) = F^*_P(\tilde{q}_m)$. This produces a PWC approximation $f^*_{\tilde{S}}$ of the prescribed stationary density f^*_P. Equations (59) and (60) imply that this may be achieved by selecting each interval $\tilde{Q}_m = (\tilde{q}_m, \tilde{q}_{m+1})$ according to

$$\tilde{q}_m = (F^*_P)^{-1}\left(\sum_{\ell=1}^{m-1}(q_{\ell+1} - q_\ell)f^*_S|_{Q_\ell}\right), \tag{61}$$

where $m = 1, 2, \ldots, M+1$. We use this expression to derive the intervals $\tilde{Q}_m$ of the required partition $\tilde{\mathcal{Q}}$. This permits the derivation of the required conjugating transform h of (55).

The PSD of the system configured to use conjugate map $\tilde{S}$ as its evolution rule has the following property.

Proposition 3: The PSD realized by $\tilde{S}$ possesses the same poles as the PSD realized by S.

Proof: As $\tilde{S}$ and S are semi-Markov maps, the poles of the PSD realized by each map coincide with the unique nonzero and nonunity (in magnitude) eigenvalues of each corresponding system's order-one FPM. However, both $\tilde{S}$ and $\tilde{S}$ are PWL hat maps, which implies that the eigenspectrum of each system's order-one FPM comprises the eigenspectrum of the system's order-zero FPM and M zero eigenvalues (Proposition 2). Thus, the poles of each system's PSD coincide with the unique nonzero and nonunity (in magnitude) eigenvalues of the system's *order-zero* FPM. Equation (57) implies that the order-zero FPMs of the systems that possess S and $\tilde{S}$ as evolution rules are similar. The proposition then follows from the fact that these matrices share the same eigenspectrum [50]. □

Proposition 3 implies that the conjugate map may be designed such that the zero-input response of its corresponding system simultaneously possesses a PDF that approximates a prescribed density *and* a PSD with prescribed poles. The poles are prescribed by selecting the eigenspectrum of the system's order-zero FPM (during the construction of the stochastic matrix in section IV-A), and the PDF is assigned by selecting the conjugating transform h of (55), where $\tilde{\mathcal{Q}}$ is selected according to (61).

D. SUMMARY OF THE NOVEL METHOD AND PARAMETER SELECTION

In this section, we summarize the novel method for system design and the approach for selecting the free parameters during each of the three design steps.

1) STEP 1: CONSTRUCTION OF A STOCHASTIC MATRIX

During the construction of the stochastic matrix in the first step, the designer selects the matrix eigenvalues to equal the non-repeating poles prescribed for the PSD, as specified by (28) and (29). These eigenvalues are inserted into the eigenspectrum of the stochastic matrix, starting with the matrix $\mathbf{P} = [1]$, in decreasing order of their modulus. The original and novel disaggregation techniques are used to insert real and strictly complex eigenvalues, respectively.

The real disaggregation technique yields the matrix $\mathbf{P}' = \mathcal{T}(\mathbf{P}, \lambda, \alpha, k)$, where the operator $\mathcal{T}$ is defined by (31) and λ denotes the real eigenvalue to be inserted into the matrix eigenspectrum. Here, the parameters $\alpha = 1/2$ and

$$k = \arg\max_{k'=1,\ldots,N} p_{k',k'} \tag{62}$$

are selected to prevent the problem of disqualifying subsequent eigenvalues from insertion into the matrix (in these expressions, $\mathbf{P} = [p_{i,j}]_{i,j=1}^N$).

The novel disaggregation technique yields the matrix $\mathbf{P}' = \mathcal{U}(\mathbf{P}, r, \theta, k)$, where the operator $\mathcal{U}$ is defined by (37). Here, the parameters $r = |\lambda|$ and $\theta = \arg(\lambda)$ are selected, where λ denotes the complex eigenvalue to be inserted into the matrix eigenspectrum. The parameter k is selected according to (62).

TABLE 1. Parameter selection for constructing systems of the first set.

Parameter	Value selected	Reason for selection
Eigenvalue λ_2 to insert in round 1.	$\lambda_2 = \kappa_1$	The parameter is selected to realize the prescribed pole κ_1.
Weight parameter α in round 1.	$\alpha = 1/2$	The parameter is selected to ensure a uniform response PDF using (35) and (36).
Index k of the matrix diagonal element to replace in round 1.	$k = 1$	The parameter is restricted to this value, as the initial matrix has a single element only.

2) STEP 2: CONSTRUCTION OF A PWL HAT MAP

In the second step, a PWL hat map S is constructed to possess the stochastic matrix from the first step as its order-zero FPM. This is achieved by specifying the map's Markov partition $\mathcal{Q}$ according to (46), the sub-partition $\mathcal{R}$ of $\mathcal{Q}$ according to (49) and (50), and each map branch according to (51) and (52). None of these expressions have any free parameters that may be specified by the designer.

3) STEP 3: TOPOLOGICAL CONJUGATION

In the third and final step, a topological conjugate $\tilde{S}$ of the PWL hat map S is constructed according to (54). Here, the conjugating transform h is defined by (55), (56) and (61). None of these expressions have any free parameters that may be specified by the designer.

V. EXAMPLES OF ELEMENTARY SYSTEMS

This section characterizes examples of elementary systems constructed using the novel method described in section IV. All of the systems were designed to generate a zero-input response with the uniform (rectangular) PDF. We investigate the systems' PSDs and describe how the structure of their maps induces the observed spectral characteristics.

Two sets of elementary systems were constructed. The systems of the first set possess Markov partitions $\mathcal{Q}$ with $M = 2$ intervals of uniform length, and were designed to possess unimodal PSDs with various mode bandwidths. The systems of the second set possess Markov partitions $\mathcal{Q}$ with $M = 3$ intervals of uniform length, and were designed to possess bimodal PSDs with distinct mode center frequencies and bandwidths. Each system of the first and second set were constructed with free parameters selected as described in section IV-D.

A. FIRST SYSTEM SET: TWO-INTERVAL PARTITION $\mathcal{Q}$

Step one of the novel method was used to derive an expression for a 2×2 stochastic matrix $\mathbf{P}_{(1)}$ with Perron eigenvalue $\lambda_1 = 1$ and a selectable eigenvalue $\lambda_2 \in (-1, 1)$. A single round of the original disaggregation technique was performed on $\mathbf{P}_{(0)} = [1]$. We select the disaggregation parameters $\lambda = \lambda_2$ and $k = 1$, as well as $\alpha = 1/2$; refer to Table 1 for details on the selection of parameter values for this step. The matrix $\mathbf{P}_{(1)}$ is given by

$$\mathbf{P}_{(1)} = \frac{1}{2}\begin{pmatrix} 1+\lambda_2 & 1-\lambda_2 \\ 1-\lambda_2 & 1+\lambda_2 \end{pmatrix}. \tag{63}$$

The choice of α leads to $\beta = 1/2$ in (36). Theorem 2 then implies that the elements of the right Perron eigenvector of $\mathbf{P}_{(1)}$ are equal, which implies that $\mathbf{P}_{(1)}$ is doubly stochastic.

Multiple doubly stochastic matrices $\mathbf{P}_{(1)}$, each having a distinct eigenvalue λ_2, were constructed using (63). Step two of the novel method was used to construct the maps S that were configured, as indicated in Fig. 1, as the systems of the first set. Each system possesses an order-zero FPM that is equal to one of the matrices $\mathbf{P}_{(1)}$. The choice of right Perron eigenvector for $\mathbf{P}_{(1)}$ leads to the uniform PDF for the system response. As the uniform density was prescribed, topological conjugation (step three of the method) was not performed.

Selecting $\lambda_2 = 0$ or $\lambda_2 = \pm 1$ leads to an order-one FPM that is not diagonalizable or not strictly positive, respectively. Hence, we do not consider these eigenvalues. Equation (26) and Proposition 2 imply that the PSD realized by S has a single pole κ_1 and at most a single zero η_1 (which is real-valued). Further investigation showed that

$$H_S(z) = \begin{cases} \dfrac{1}{z-\kappa_1}, & \text{if } \lambda_2 = \zeta \\ \dfrac{z-\eta_1}{z-\kappa_1}, & \text{if } \lambda_2 \in (-1,1) \setminus \{0, \zeta\}, \end{cases} \tag{64}$$

where $\kappa_1 = \lambda_2$ and $\zeta \triangleq -1/3 + \sqrt{10/9} \approx 0.721$. Thus, the zero η_1 disappears if $\lambda_2 = \zeta$ is selected. The pole and zero are plotted as functions of λ_2 in Fig. 5(a). The pole and zero were found to cancel if $\lambda_2 = 1 - \sqrt{2} \approx -0.414$ is selected.

The PSDs of the systems that were constructed with eigenvalue λ_2 selected from $\{\pm 0.1, \pm 0.3, \pm 0.5, \pm 0.7, \pm 0.9\}$ are plotted in Fig. 5(b) and Fig. 5(c). In these figures, solid lines represent the values computed by evaluating the theoretical expression for the PSD, and the dots represent values computed numerically to verify the results predicted by theory. The numerical results were obtained by simulating each system digitally and directly computing the statistics from the zero-input response generated by the system.

Recall that the selection of a positive or negative real eigenvalue λ_2 leads to the realization of a spectral mode with center frequency equal to zero or π radians per sample, respectively (stated differently, a pole equal to the eigenvalue is realized). The figures show that the spectral modes associated with eigenvalues $\lambda_2 > 1 - \sqrt{2} \approx -0.414$ appear as peaks centered at zero radians per sample in the PSDs. This coincides with the zero η_1 appearing to the left-hand side of the pole κ_1, on the real line in the z-plane, for these values of λ_2 (as implied by Fig. 5(a)). As progressively smaller eigenvalues $\lambda_2 > 1 - \sqrt{2}$ are selected, the peak is lowered and its bandwidth becomes wider.

Selecting $\lambda_2 = 1 - \sqrt{2} \approx -0.414$ causes the pole and zero to cancel each other, thereby leading to a flat PSD. The systems associated with eigenvalues $\lambda_2 < 1 - \sqrt{2}$ possess PSDs with a peak centered at π radians per sample, which is

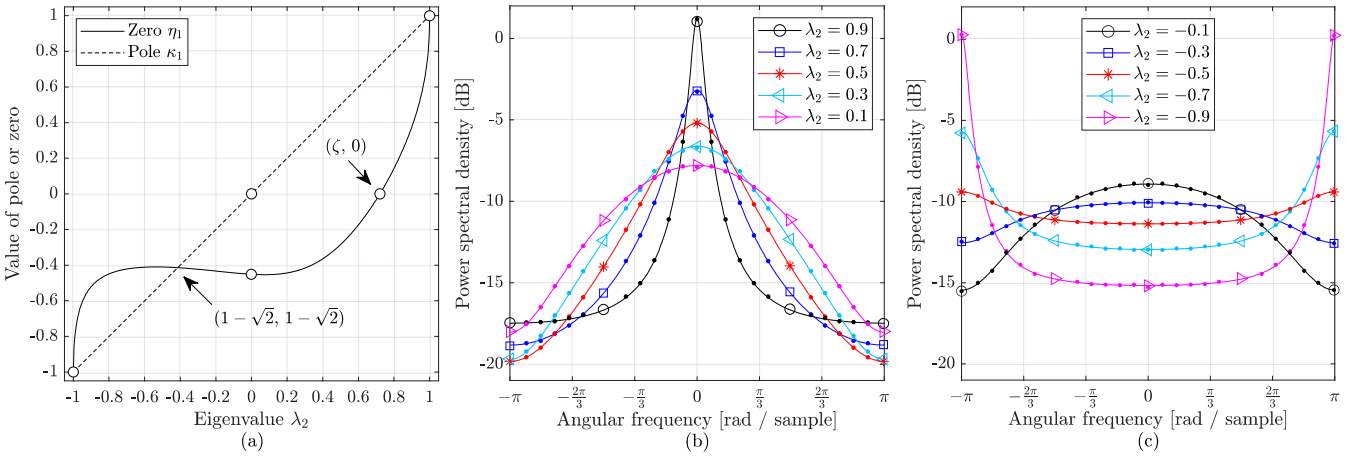


FIGURE 5. Plots of (a) the PSD pole and zero of the systems belonging to the first set, as a function of eigenvalue λ_2, where circles represent excluded values, and (b) and (c) the PSDs of the systems from this set, for positive and negative eigenvalues λ_2, respectively. In (b) and (c), solid lines represent values computed by evaluating the theoretical expressions and dots represent values computed using numerical simulation to verify the results predicted by theory.

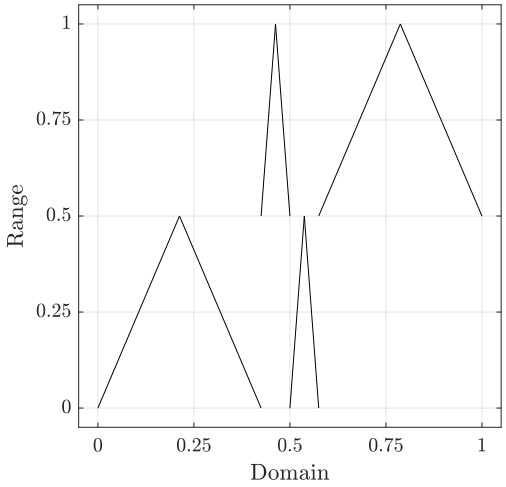


FIGURE 6. Plot of the hat map associated with the first set of systems and which realizes an order-zero FPM with the eigenvalue $\lambda_2 = 0.7$.

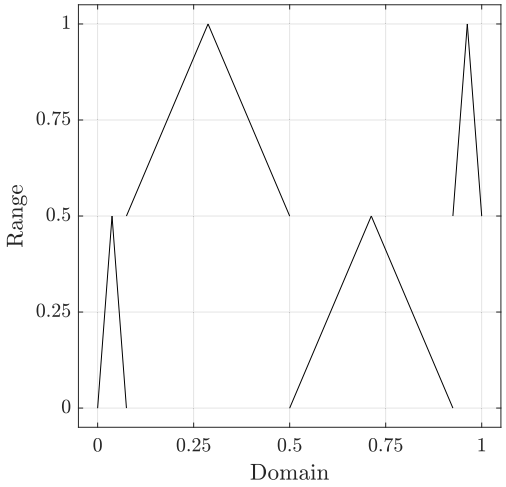


FIGURE 7. Plot of the hat map associated with the first set of systems and which realizes an order-zero FPM with the eigenvalue $\lambda_2 = -0.7$.

equal to the center frequency of the spectral mode associated with λ_2. The appearance of this peak coincides with the zero η_1 now appearing to the right-hand side of the pole κ_2 on the real line in the z-plane. As $\lambda_2 < 1 - \sqrt{2}$ becomes progressively smaller, the peak is elevated and its bandwidth becomes narrower.

Figs. 5(b) and 5(c) reveal that the PSDs computed using numerical simulation closely approximate the PSDs predicted by theory. This also verifies that the PSD of the system response agrees with the PSD prescribed during the design of each system.

The hat maps constructed with eigenvalues $\lambda_2 = 0.7$ and $\lambda_2 = -0.7$ are plotted in Fig. 6 and Fig. 7, respectively. Each of these maps possesses two pairs of hats. The hats of each pair have equally wide support; we describe the hats of each pair as *wider* or *narrower* based on the relative width of their support. In the map associated with $\lambda_2 = 0.7$, the wider hats map system states from interval Q_1 or Q_2 back to the same interval from one time instant to the next. This is a characteristic of maps associated with positive eigenvalues λ_2. However, in the map associated with $\lambda_2 = -0.7$, the wider hats map states from interval Q_1 to Q_2 (and vice versa) from one time instant to the next. Maps associated with negative eigenvalues λ_2 possess this characteristic. The disparity in the width of each map's wider and narrower hats grows as $|\lambda_2|$ increases.

There exists a relationship between the disparity in hat width referred to above and the PSD characteristics of the corresponding systems. Consider the evolution of the uniform (stationary) state density of the systems configured to use the maps plotted in Fig. 6 and Fig. 7 as evolution rules. In this *stationary regime*, the Borel measure of those states mapped from one time instant to the next by the wider hats is larger than the Borel measure of those mapped by the narrower hats in proportion to the disparity in hat width. As the wider hats of Fig. 6 (where $\lambda_2 = 0.7$) map states from Q_1 or Q_2 back to the same interval, the dominant behavior of the zero-input response generated by this system in the stationary regime

is to remain in the same interval Q_1 or Q_2 from one time instant to the next. This *slower* response behavior gives rise to the observed PSD peak centered at zero radians per sample (refer to Fig. 5(b)). In contrast, the wider hats of Fig. 7 (where $\lambda_2 = -0.7$) map states from Q_1 to Q_2 and vice versa. The dominant behavior of the response generated by this system in the stationary regime is to rapidly move back and forth between the partition intervals. This *faster* behavior gives rise to the observed PSD peak centered at π radians per sample (refer to Fig. 5(c)). As $|\lambda_2|$ increases, the disparity in hat width grows, the dominant behavior of the response intensifies, and a higher PSD peak is realized.

B. SECOND SYSTEM SET: THREE-INTERVAL PARTITION $\mathcal{Q}$

Step one of the novel method was used to derive an expression for a 3×3 stochastic matrix $\mathbf{P}_{(1)}$ with Perron eigenvalue $\lambda_1 = 1$ and a selectable pair of strictly complex eigenvalues λ_2 and $\lambda_3 = \lambda_2^*$. A single round of the novel disaggregation technique was performed on $\mathbf{P}_{(0)} = [1]$. By using this technique, the region of permissible values that λ_2 may assume is the interior of the black triangle in the complex plane of Fig. 8(a), but with the real line excluded. *All* pairs of strictly complex eigenvalues that may belong to a 3×3 doubly stochastic matrix, and where the eigenvalue modulus is strictly less than unity, lies within this region [89].

We derive the expression for the stochastic matrix with the disaggregation parameters $r = |\lambda_2|$ and $\theta = \arg(\lambda_2)$; refer to Table 2 for details on the selection of parameter values for this step. The matrix is then given by $\mathbf{P}_{(1)} = U(1, r, \theta)$, where U is defined in (38) to (41). Theorem 2 implies that the elements of the right Perron eigenvector of $\mathbf{P}_{(1)}$ are equal, which implies that each matrix $\mathbf{P}_{(1)}$ is doubly stochastic.

Specific pairs of eigenvalues were selected from the region of permissible values by defining two loci, which correspond to the concentric blue and red triangles in Fig. 8(a). Those points on the loci denoted by blue and red markers (i.e., on the top half of each triangle) were prescribed as eigenvalues λ_2 for the matrices that were constructed; these eigenvalues are listed in Table 3. The markers also lie on radial lines of the unit circle that form angles of $k\pi/6$ radians with the real line, where $k = 1, 2, \ldots, 5$. This implies that the eigenvalues λ_2 denoted by the markers satisfy $\arg(\lambda_2) = k\pi/6$. The corresponding eigenvalues λ_3 are denoted by gray markers. We use Λ to denote the set of all eigenvalues represented by the markers of Fig. 8(a), regardless of the marker's color.

Multiple doubly stochastic matrices $\mathbf{P}_{(1)}$, each possessing a distinct pair of eigenvalues as selected above, were constructed using (38). Step two of the novel method was used to construct the maps S that were configured, as indicated in Fig. 1, as the systems of the second set. Each system possesses an order-zero FPM that is equal to one of the matrices $\mathbf{P}_{(1)}$. The right Perron eigenvector of $\mathbf{P}_{(1)}$ leads to almost every zero-input response of each system possessing the prescribed uniform (rectangular) PDF. Topological conjugation was therefore not necessary and omitted.

The PSDs of the systems in the second set are plotted in Fig. 8(b) and Fig. 8(c) for those cases where λ_2 coincides with the blue and red markers of Fig. 8(a), respectively. In these figures, solid lines represent values computed by evaluating the theoretical expression for the PSD, and the dots represent values computed numerically as verification; the latter were again obtained by simulating the systems digitally. Equation (26) and Proposition 2 imply that the PSD of each system has two poles and at most two zeros. The poles and zeros appear as complex conjugate pairs. In particular,

$$H_S(z) = \frac{(z - \eta_1)(z - \eta_2)}{(z - \kappa_1)(z - \kappa_2)}, \qquad \lambda_2 \in \Lambda, \tag{65}$$

where $\kappa_1 = \lambda_2$ and $\kappa_2 = \lambda_3 = \lambda_2^*$. The poles and zeros of each PSD in Figs. 8(b) and 8(c) are plotted in Figs. 9(a) to 9(j). These pole-zero plots indicate the location of the poles and zeros of each PSD in the complex plane, thus aiding the interpretation of the PSDs in Figs. 8(b) and 8(c). More specifically, as a pole or zero approaches the unit circle in the complex plane, the PSD will exhibit a growing peak or valley at the angular frequency that coincides with the argument of the pole or zero, respectively.

Recall that each eigenvalue λ_2 and λ_3 coincides with a pole of the PSD, and thus leads to the realization of a spectral mode with center frequency equal to the eigenvalue's argument. Since λ_3 is predetermined as the complex conjugate of λ_2 during disaggregation, two spectral modes with center frequencies of $\pm\arg(\lambda_2)$ radians per sample are realized for each system. The two spectral modes associated with the selection of $\arg(\lambda_2) = \pi/6$ appear as a single peak centered at zero radians per sample in the corresponding PSD of Fig. 8(b). This PSD is associated with the pole-zero plot of Fig. 9(a). As $\arg(\lambda_2)$ increases from $2\pi/6$ to $4\pi/6$, Figs. 9(b) to 9(d) reveal that the poles associated with λ_2 and λ_3 move apart and closer to the unit circle. The spectral modes associated with λ_2 and λ_3 are thus distinguishable as separate peaks in the corresponding PSDs of Fig. 8(b). The poles reach their closest point to the unit circle when $\arg(\lambda_2) = 4\pi/6$, which corresponds with the PSD having two elevated and narrow peaks centered at frequencies of approximately $\pm 4\pi/6$ radians per sample. The PSD associated with $\arg(\lambda_2) = 5\pi/6$ and appearing in Fig. 8(b) has significantly lower and wider peaks when compared to the preceding PSDs. Fig. 9(e) reveals that, in this case, the poles and zeros are closer to one another in the z-plane, relative to their distance from the unit circle.

The PSDs of the systems associated with eigenvalues λ_2 denoted by the red markers of Fig. 8(a) are plotted in Fig. 8(c). The figure shows that these PSDs have similar characteristics to those plotted in Fig. 8(b), except that the power ratio between the peak(s) and the valley of each PSD is significantly smaller and the bandwidths of the peaks are wider. Figs. 9(f) to 9(j) imply that this is due to each PSD's poles and zeros being located closer to one another and further from the unit circle in the z-plane, as compared to the pole-zero plots of Figs. 9(a) to 9(e).

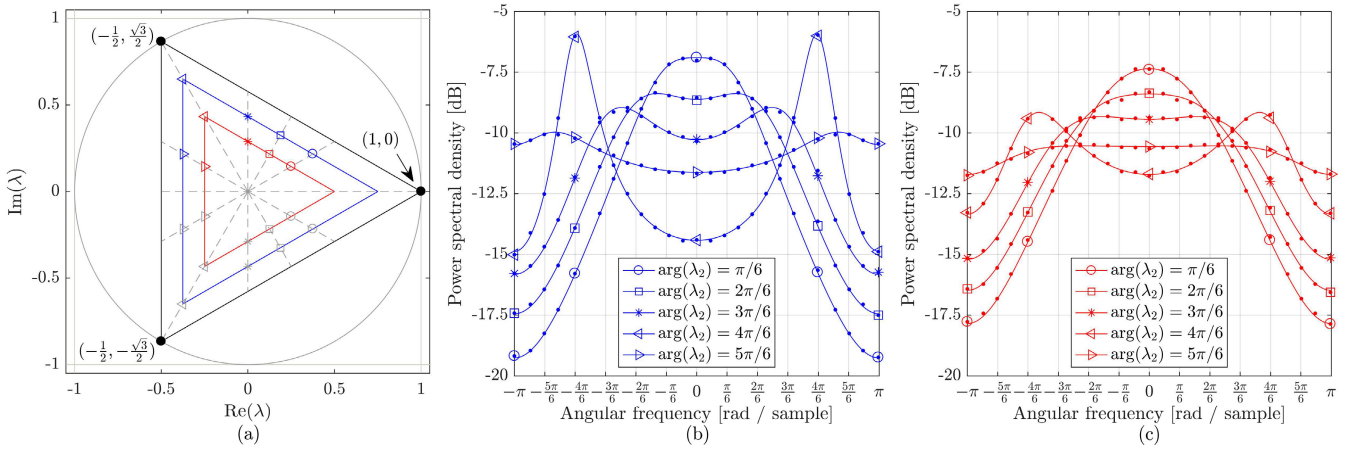


FIGURE 8. Plots of (a) the region of permissible eigenvalues λ_2 associated with the systems of the second set, where blue and red markers denote those eigenvalues selected, and (b) and (c) the PSDs of the systems from this set, for eigenvalues λ_2 denoted by the blue and red markers in (a), respectively. In (b) and (c), solid lines represent values computed by evaluating the theoretical expressions and dots represent values computed using numerical simulation to verify the results predicted by theory.

TABLE 2. Parameter selection for constructing systems of the second set.

Parameter	Value selected	Reason for selection
Modulus r of the eigenvalues λ_2, λ_3 to insert in round 1.	$r = \lvert\kappa_1\rvert$ $= \lvert\kappa_2\rvert$	The parameter is selected to realize the prescribed poles κ_1, κ_2.
Argument θ of the eigenvalue λ_2 to insert in round 1.	$\theta = \arg(\kappa_1)$ $= -\arg(\kappa_2)$	The parameter is selected to realize the prescribed poles κ_1, κ_2.
Index k of the matrix diagonal element to replace in round 1.	$k = 1$	The parameter is restricted to this value, as the initial matrix has a single element only.

In the examples presented above, we have demonstrated the ability to independently adjust the center frequency and bandwidth of the spectral modes using the proposed method. In particular, by independently selecting the argument and the modulus of eigenvalue λ_2 during the design of the system, the center frequencies of the two modes may be selected and their bandwidth adjusted. Furthermore, Figs. 8(b) and 8(c) demonstrate that the PSDs computed using numerical simulation closely approximate the PSDs predicted by theory. This verifies that the PSD of the system response agrees with the PSD prescribed during the design of each system.

The map associated with eigenvalue $\lambda_2 = 0.75\exp(i4\pi/6)$, which is located on the blue triangle of Fig. 8(a), is plotted in Fig. 10. The map possesses nine hats, where three of the hats have equal but significantly wider support than the remaining hats. These *wider hats* map states from one interval to the next in the repeating pattern $Q_1 \to Q_3 \to Q_2 \to Q_1 \to \ldots$. This observation reveals a relationship between the map's structure and the PSD of the system's zero-input response. Using the same argument as that presented in section V-A, we find that the dominant behavior of the response generated by the system in the stationary regime is to move between the intervals in the repeating pattern. The pattern has a period of 3 samples, and thus an angular frequency of $\omega = 4\pi/6$ radians per sample. This frequency coincides with the center frequency of the spectral mode associated with λ_2. This spectral mode appears as a sharp peak in the corresponding PSD of Fig. 8(b).

TABLE 3. Eigenvalues λ_2 denoted by the markers in Fig. 8(a).

Marker	○	□	✳	◁	▷
$r = \lvert\lambda_2\rvert$	0.433	0.375	0.433	0.750	0.433
$\theta = \arg(\lambda_2)$	$\pi/6$	$2\pi/6$	$3\pi/6$	$4\pi/6$	$5\pi/6$

Marker	○	□	✳	◁	▷
$r = \lvert\lambda_2\rvert$	0.289	0.250	0.289	0.500	0.289
$\theta = \arg(\lambda_2)$	$\pi/6$	$2\pi/6$	$3\pi/6$	$4\pi/6$	$5\pi/6$

VI. EXAMPLES OF SOPHISTICATED SYSTEMS

In section VI-A, more sophisticated systems with richer statistical metrics (PDF and PSD) are constructed using the novel analytical method and characterized. The potential of using existing analytical methods to construct systems with the same statistical metrics is evaluated in section VI-B. A final example, where the novel method is used to construct two systems that yield increasingly accurate approximations of a prescribed zero-input response PDF that is smooth, is presented in section VI-C.

A. THE NOVEL METHOD

The novel method was used to construct systems that generate a zero-input response with a PDF that approximates the prescribed beta PDF

$$f_P^*(x) = \frac{x^{a-1}(1-x)^{b-1}}{B(a,b)}, \qquad x \in (0,1), \tag{66}$$

with parameters $a = 3/2$ and $b = 5/2$, where

$$B(a,b) \triangleq \frac{\Gamma(a)\Gamma(b)}{\Gamma(a+b)} \tag{67}$$

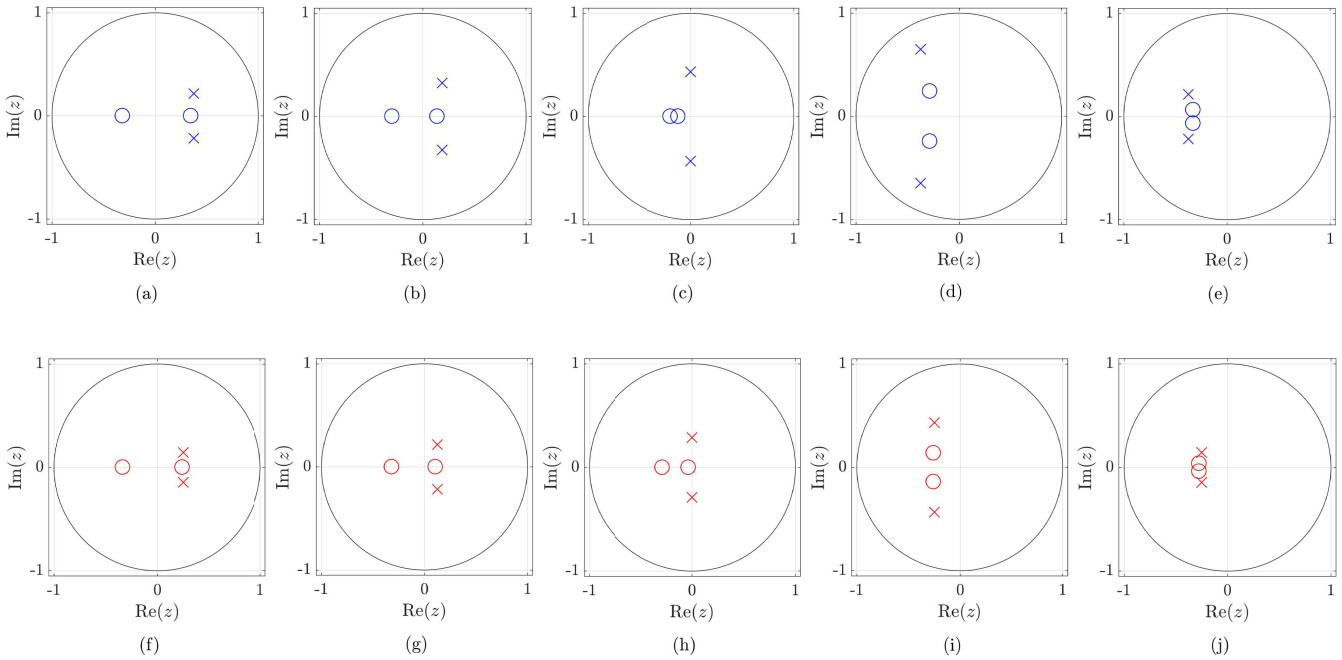


FIGURE 9. Pole-zero plots associated with the systems of the second set. In these plots, crosses represent poles and circles represent zeros. Plots (a) to (e) and plots (f) to (j) are associated with eigenvalues λ_2 denoted by the blue and red markers of Fig. 8(a), respectively. From left to right, the pole-zero plots of each row correspond to $\arg(\lambda_2) = \pi/6, 2\pi/6, \ldots, 5\pi/6$.

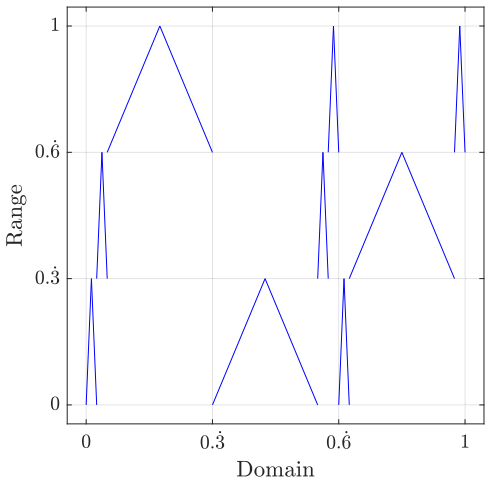


FIGURE 10. Plot of the hat map associated with the second set of systems that realizes an order-zero FPM with eigenvalue $\lambda_2 = 0.75\exp(i4\pi/6)$.

and $\Gamma(a) \triangleq \int_0^\infty x^{a-1}e^{-x}dx$. The prescribed PDF is plotted in Fig. 11(b) (black curve). Three PSD poles given by

$$\begin{aligned}\kappa_1 &= 3/4\\ \kappa_2 &= \kappa_3^* = r\exp(i2\pi/3),\end{aligned} \tag{68}$$

were prescribed for each system. Parameter values of $r \in \{0.3, 0.5, 0.7, 0.9\}$ were selected to construct systems that possess distinct maps.

Step one of the novel method was used to derive an expression for a 4×4 stochastic matrix with eigenvalues $\lambda_1 = 1$ and $\lambda_k = \kappa_{k-1}$, where $k = 2, 3, 4$. A single round of original disaggregation was performed on $\mathbf{P}_{(0)} = [1]$ to insert eigenvalue $\lambda_2 = 3/4$ into its eigenspectrum, thereby generating $\mathbf{P}_{(1)}$ (refer to Table 4 for details on the selection of parameter values for this example). We specify the right Perron eigenvector $\boldsymbol{\pi}_{(1)} = [3/4, 1/4]^T$ for $\mathbf{P}_{(1)}$. To construct $\mathbf{P}_{(1)}$, the disaggregation parameters $\lambda = 3/4$, $k = 1$ and $\alpha = 15/28$ were selected (the latter was obtained by solving (36) for α, where $\beta = 3/4$). Hence, $\mathbf{P}_{(1)} = T(1, \lambda, \alpha)$, where T is given by (32).

A single round of novel disaggregation was performed on $\mathbf{P}_{(1)}$ to insert the eigenvalues $\lambda_2 = r\exp(i2\pi/3)$ and $\lambda_3 = \lambda_2^*$ into its eigenspectrum, thereby generating $\mathbf{P}_{(2)}$. The disaggregation parameters $\theta = 2\pi/3$ and $k = 1$ yield

$$\mathbf{P}_{(2)} = \frac{1}{48}\begin{pmatrix} 15-16r & 15+32r & 15-16r & 3\\ 15-16r & 15-16r & 15+32r & 3\\ 15+32r & 15-16r & 15-16r & 3\\ 3 & 3 & 3 & 39\end{pmatrix}, \tag{69}$$

where $0 < r < 15/16$. $\mathbf{P}_{(2)}$ has a right Perron eigenvector with equal elements (Theorem 2) and is doubly stochastic.

Step two of the novel method was used to construct multiple maps S that realize an order-zero FPM equal to $\mathbf{P}_{(2)}$. We observe that the right Perron eigenvector of each matrix $\mathbf{P}_{(2)}$ implies that a system configured to use any map S generates a zero-input response with a uniform (rectangular) PDF. Step three (topological conjugation) was thus performed to construct systems with a response PDF that approximates the prescribed beta PDF. Each conjugate map $\tilde{S} \triangleq h \circ S \circ h^{-1}$ has the Markov partition $\tilde{\mathcal{Q}} = \{\tilde{Q}_m\}_{m=1}^4$, where $\tilde{Q}_m \triangleq (\tilde{q}_m, \tilde{q}_{m+1})$. The partition points were derived using (61), and are given by $\tilde{q}_1 = 0$, $\tilde{q}_2 \approx 0.199$, $\tilde{q}_3 \approx 0.352$, $\tilde{q}_4 \approx 0.531$ and $\tilde{q}_5 = 1$. The maps share the same conjugating

TABLE 4. Parameter selection for constructing the sophisticated systems.

Parameter	Value selected	Reason for selection
Eigenvalue λ_2 to insert in round 1.	$\lambda_2 = \kappa_1$	The parameter is selected to realize the prescribed pole $\kappa_1 = 3/4$.
Weight parameter α in round 1.	$\alpha = 15/28$	The parameter is selected to ensure a uniform response PDF after the second round of disaggregation, and prior to topological conjugation. More specifically, the weight parameter is selected to yield a right Perron eigenvector $\boldsymbol{\pi}_{(1)} = [3/4, 1/4]^T$ after the first round of disaggregation, using (35) and (36). The first element of this eigenvector is necessary divided into three equal values after the second round of disaggregation (using the novel disaggregation technique; refer to Theorem IV.3), which then yields the uniform PDF.
Index k of the matrix diagonal element to replace in round 1.	$k = 1$	The parameter is restricted to this value, as the initial matrix has a single element only.
Modulus r of the eigenvalues λ_3, λ_4 to insert in round 2.	$r = \lvert\kappa_2\rvert$ $= \lvert\kappa_3\rvert$	The parameter is selected to realize the prescribed poles κ_2, κ_3.
Argument θ of the eigenvalue λ_3 to insert in round 2.	$\theta = \arg(\kappa_2)$ $= -\arg(\kappa_3)$	The parameter is selected to realize the prescribed poles κ_2, κ_3.
Index k of the matrix diagonal element to replace in round 2.	$k = 1$	The parameter is selected to yield the uniform PDF according to (45).

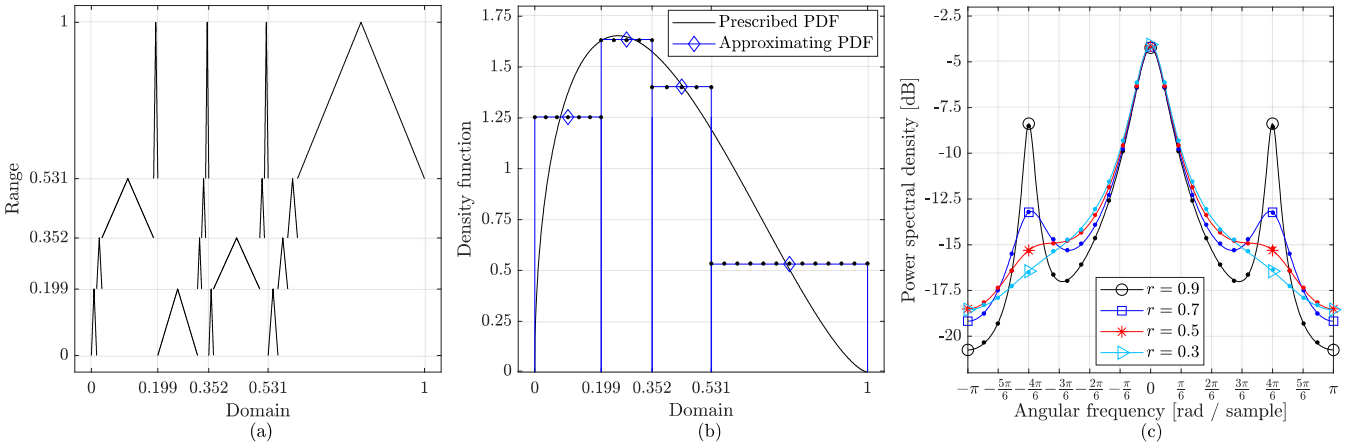


FIGURE 11. Plots associated with the examples of section VI-A. These plots are (a) the conjugate map $\tilde{S}$ associated with $r = 0.7$, (b) the prescribed response PDF (black) and the response PDF shared by all systems that use the conjugate maps $\tilde{S}$ (blue), and (c) the PSDs of the systems that use the conjugate maps $\tilde{S}$. In (b) and (c), solid lines represent values computed by evaluating the theoretical expressions and dots represent values computed using numerical simulation to verify the results predicted by theory.

transform h of (55), where $q_m = (m-1)/4$. The systems that use these maps were configured as indicated in Fig. 1.

The results obtained for this example are plotted in Fig. 11. In this figure, solid lines represent the theoretical expressions, and the dots represent values computed numerically from the zero-input response generated by the system. The conjugate map $\tilde{S}$ associated with $r = 0.7$ is plotted in Fig. 11(a). We observe that interval $\tilde{Q}_4$ of the map's Markov partition $\tilde{\mathcal{Q}}$ is significantly longer than its remaining intervals. The map possesses sixteen hats and four of the hats have significantly wider support than the remaining hats.

The zero-input response PDF shared by all systems that use the conjugate maps $\tilde{S}$ is plotted in blue in Fig. 11(b). This density function is a PWC approximation of the prescribed PDF over $\tilde{\mathcal{Q}}$. By using h of (55), the approximation is realized such that the areas under both densities over each interval $\tilde{Q}_m$ are equal. The disproportionate length of $\tilde{Q}_4$ is thus due to the steeply descending slope of the prescribed density function over this interval. The figure also demonstrates that the numerical simulations yielded a response PDF that closely approximates the PWC PDF predicted by theory.

The PSDs of the systems that were configured to use the conjugate maps $\tilde{S}$ are plotted in Fig. 11(c). We do not characterize the zeros of each system's PSD in this paper. However, Proposition 3 implies that each map S and its conjugate $\tilde{S}$ realize systems with identical PSD poles. The prescribed poles thus lead to the realization of three spectral modes with center frequencies $\arg(\kappa_1) = 0$ and $\arg(\kappa_2) = -\arg(\kappa_3) = 2\pi/3$ radians per sample. As r increases, these spectral modes begin to appear as peaks in the PSD at their center frequencies. These peaks are elevated as progressively larger values of r are selected, due to the poles moving closer to the unit circle in the z-plane.

Fig. 11(c) demonstrates that the PSDs computed using numerical simulation closely approximate the PSDs predicted by theory and as prescribed during system design.

B. EXISTING METHODS

We investigate the use of existing analytical methods to construct systems that share the prescribed zero-input response PDF of (66) and possess exactly three prescribable

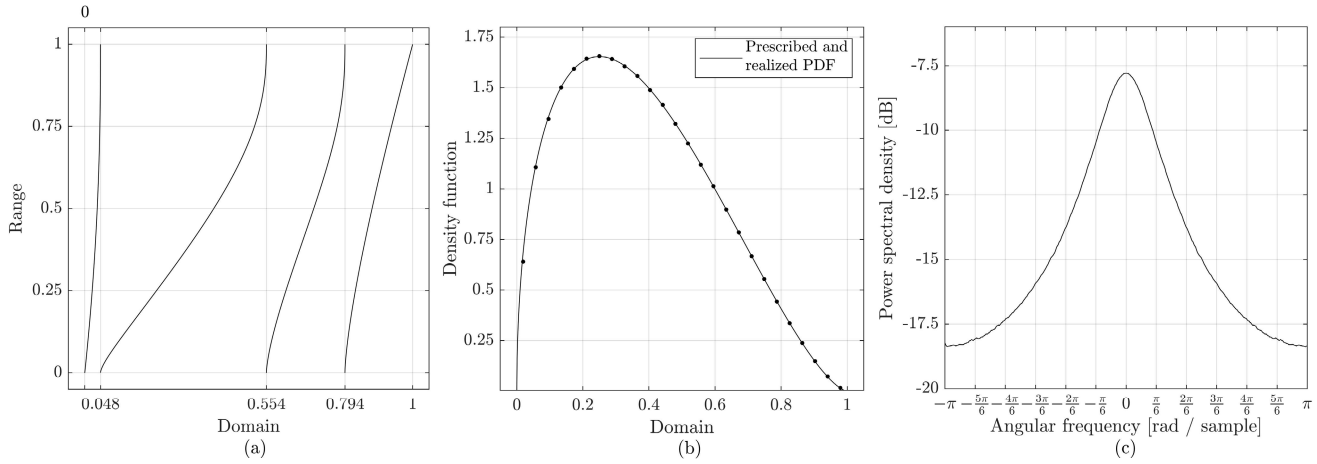


FIGURE 12. Plots associated with the system designed using the topological conjugation method of [12]. These plots are (a) the map used by the system, (b) the prescribed and realized response PDF associated with the system, and (c) the PSD of the system response, computed numerically. In (b), dots represent values computed using numerical simulation to verify the results predicted by theory.

PSD poles. The poles are to be selected according to (68). We refer to these as the *required systems* in what follows.

The topological conjugation method, as developed in [12], only permits construction of topological conjugates of complete and piecewise-monotonic maps while simultaneously affording the freedom to select the system's single spectral mode. Systems configured to use these conjugate maps possess a PSD with at most a single pole. Hence, this method is disqualified from realizing the required systems. However, in contrast to the novel method proposed in this paper, the method of [12] may construct a system with a zero-input response that has a PDF *equal* to the prescribed beta density of (66). The latter method is more flexible in this regard.

The topological conjugation method of [12] was used to design a system with a prescribed response PDF given by (66), as well as a prescribed PSD comprising a single spectral mode with a center frequency of zero radians per sample. The map used by the system is plotted in Fig. 12(a). The map has four branches with positive slope, each spanning the full codomain of the map. The prescribed PDF and the realized response PDF are plotted in Fig. 12(b). This figure shows that the response PDF coincides with the prescribed PDF. The numerically-computed PSD of the system, as plotted in Fig. 12(c), has a single spectral mode with a peak of zero radians per sample. This example highlights the restricted nature of the method proposed in [12]; i.e., it cannot realize more than one spectral mode. In contrast, the novel method permits the realization of an arbitrary number of spectral modes, where the center frequency of each mode is specifiable.

The method proposed in [40] may be used to construct systems that possess a PSD with at most $2M-1$ poles, of which at most $M-1$ are prescribable as real values (here, $M>1$ is a parameter that may be selected). As the required systems possess PSDs with complex-valued poles, this method is also disqualified from realizing the required systems. However, similar to the novel method proposed in this paper, the method of [40] permits the PWC approximation of the prescribed response PDF.

Although the method of [41] may construct systems with PSDs that possess complex-valued poles, it only permits construction of systems that possess at most five poles, of which at most two are prescribable. As the required systems possess three prescribed poles, the method is disqualified from realizing the required systems. Also, the method can only realize a system response with a PDF that is uniform over the unit interval.

Finally, we consider the matrix method of [69], [70], [71], and [72], as described in the final paragraph of section III. It was shown in [70] that the eigenvalues of this matrix are restricted to being real-valued and strictly positive. Hence, any method that realizes this matrix as a system's order-zero FPM cannot construct the required systems, regardless of the particulars of the method. However, this method permits the PWC approximation of the prescribed zero-input response PDF in a fashion similar to the proposed method.

C. APPROXIMATION OF A PRESCRIBED SMOOTH RESPONSE PDF

In this example, two systems are constructed to possess zero-input response PDFs that approximate the beta PDF defined in (66) with parameters $a=2$ and $b=3$ (the latter PDF is plotted in blue in Fig. 13 and Fig. 14). The two systems are constructed to possess 15 and 31 real-valued poles uniformly spaced over the interval $[-0.1, 0.15]$, respectively. The poles prescribed for system one are

$$\kappa_m = 0.15 - \frac{m-1}{56}, \qquad m = 1, 2, \ldots, 15, \tag{70}$$

and the poles prescribed for system two are

$$\kappa_m = 0.15 - \frac{m-1}{120}, \qquad m = 1, 2, \ldots, 31. \tag{71}$$

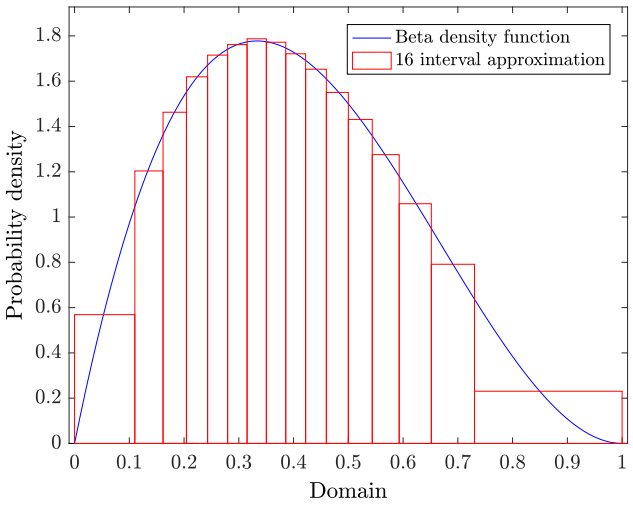


FIGURE 13. Prescribed zero-input response PDF (plotted in blue) and the response PDF realized with the first system of the example of section VI-C (plotted in red), for a Markov partition of 16 intervals [40].

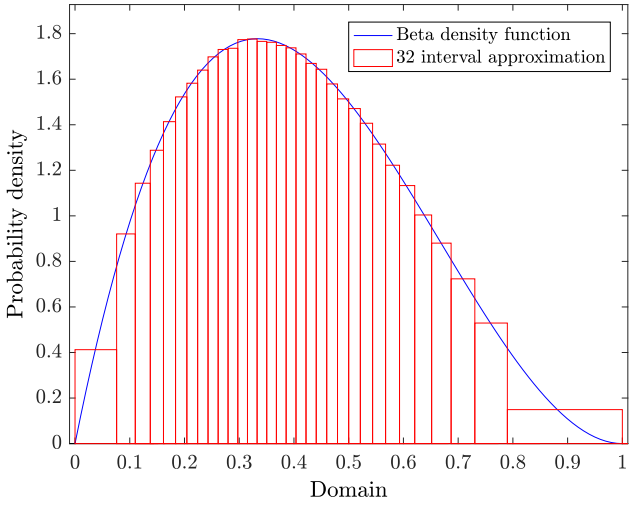


FIGURE 14. Prescribed zero-input response PDF (plotted in blue) and the response PDF realized with the second system of the example of section VI-C (plotted in red), for a Markov partition of 32 intervals [40].

The two systems are constructed using the novel method by performing 15 and 31 rounds of the original disaggregation technique on the matrix $\mathbf{P}_{(0)} = [1]$, respectively. The poles are inserted as eigenvalues into the order-zero FPM for each system, from the largest to the smallest eigenvalue. During each round m of disaggregation, the largest diagonal element of the matrix $p_{k,k}$ is replaced with the relevant 2×2 matrix given by (32), with parameters $\alpha = 1/2$ and $\lambda = \kappa_m$.

The above systems possess zero-input response PDFs that are PWC approximations of the beta PDF over Markov partitions of 16 and 32 intervals. These response PDFs are plotted in Fig. 13 and Fig. 14 (red curves). These figures show that the increase in the interval count yields a more accurate approximation of the beta PDF. In particular, the root-mean-square error between the response PDF and the prescribed beta PDF decreases from $\varepsilon \approx 0.149$ for the approximation over the Markov partition with 16 intervals to $\varepsilon \approx 0.090$ for the approximation over the Markov partition with 32 intervals. This demonstrates the potential of the novel method to generate systems with zero-input response PDFs that are increasingly accurate approximations of a prescribed smooth response PDF.

VII. CONCLUSION

This paper presents a novel analytical method for designing an ergodic discrete-time dynamical system that generates a zero-input response which satisfies prescribed statistical metrics as specifications. The hat-like structure of the system's evolution rule permits the simultaneous prescription of the PDF belonging to the system's zero-input response and the poles of its PSD. Unlike existing methods, the novel method

- does not rely on a numerical search to minimize a cost function during system design and is thus immune to possible non-convergence,
- affords the freedom to *arbitrarily select* the number of PSD poles and to prescribe *all* of these poles as a set of non-repeating *complex values*, and
- permits expressions that qualify whether a set of complex values is realizable as the PSD poles of the system to be constructed.

Using the novel method, we constructed examples of elementary systems that generate a zero-input response with the uniform (rectangular) PDF in conjunction with PSDs possessing up to two poles. These systems were characterized and their structural features that give rise to the observed spectral characteristics were identified. Additional examples that illustrate the method's ability to construct systems with richer statistical metrics were provided, and it was shown that more than two PSD peaks are realizable using the method.

Although the novel method does not provide a means for selecting the zeros of the system's PSD, the designer may manipulate the properties of the spectral modes by selecting the power spectrum poles. In particular, the independent adjustment of the center frequencies and bandwidths of the peaks in the power spectrum was demonstrated. Furthermore, whereas the PWC nature of the PDF realized as the system response can only approximate arbitrary nonuniform densities, an example was presented where the novel method was used to construct systems with response PDFs that are increasingly accurate approximations of a prescribed smooth PDF. This further demonstrates the novel method's versatility.

It is anticipated that the corresponding systems will find immediate application in the area of low-complexity random signal generation due to the piecewise-linear nature of their evolution rules and the richness of their power spectra. In particular, the systems constructed using the new method may be considered for use as efficient random signal generators for Monte Carlo simulation in domains such as mobile communications and radar engineering. We also anticipate that systems constructed using the novel method will find application in DRFM hardware-in-the-loop systems

for radar performance evaluation, which require real-time low-complexity random signal generation techniques that afford as much freedom as possible to prescribe the signals' PDF and PSD.

VIII. FUTURE WORK

The performance evaluation of random signal generators that utilize systems constructed using the novel method, and the generalization of the novel method to provide a means for specifying the zeros of the system's PSD, are topics for future work. A further topic for investigation is the application of the hat maps towards probabilistic analysis and modeling problems outside the context of the IFPP. In particular, these maps may be used to construct approximations to singular maps that may permit their asymptotic analysis.

Particularly interesting future work, somewhat removed from possible extensions of the work reported herein, pertains to the Frobenius-Perron operator equation itself. First, as infinite-dimensional iterative linear systems are able to exhibit chaos given appropriate conditions [90], the question arises as to whether iterates of the Frobenius-Perron equation can exhibit chaos. This could shed light on possible complications that might arise during numerical simulations of chaotic systems in general. Second, and somewhat esoteric, is the notion of the Frobenius-Perron equation converted to a stochastic integral such as the Ito integral, its meaning, and possible applications.

REFERENCES

[1] W. Hörmann, J. Leydold, and G. Derflinger, *Automatic Nonuniform Random Variate Generation*, 1st ed., Berlin, Germany: Springer, 2004, doi: 10.1007/978-3-662-05946-3.

[2] G. Q. Cai, "Generation of correlated random variables and stochastic processes," *Probabilistic Eng. Mech.*, vol. 52, pp. 40–46, Apr. 2018, doi: 10.1016/j.probengmech.2018.03.003.

[3] C. Maggi, N. Gnan, M. Paoluzzi, E. Zaccarelli, and A. Crisanti, "Critical active dynamics is captured by a colored-noise driven field theory," *Commun. Phys.*, vol. 5, no. 1, pp. 1–10, Mar. 2022, doi: 10.1038/s42005-022-00830-5.

[4] R. Srikanthan and T. A. McMahon, "Stochastic generation of annual, monthly and daily climate data: A review," *Hydrol. Earth Syst. Sci.*, vol. 5, no. 4, pp. 653–670, Dec. 2001, doi: 10.5194/hess-5-653-2001.

[5] T. R. Beal, "Digital simulation of atmospheric turbulence for Dryden and von Karman models," *J. Guid., Control, Dyn.*, vol. 16, no. 1, pp. 132–138, Jan. 1993, doi: 10.2514/3.11437.

[6] U. Gujar and R. Kavanagh, "Generation of random signals with specified probability density functions and power density spectra," *IEEE Trans. Autom. Control*, vol. AC-13, no. 6, pp. 716–719, Dec. 1968, doi: 10.1109/TAC.1968.1099062.

[7] R. M. May, "Simple mathematical models with very complicated dynamics," *Nature*, vol. 261, no. 5560, pp. 459–467, Jun. 1976, doi: 10.1038/261459a0.

[8] A. Boyarsky and P. Góra, *Laws of Chaos: Invariant Measures and Dynamical Systems in One Dimension*, 1st ed., Boston, MA, USA: Birkhäuser, 1997, doi: 10.1007/978-1-4612-2024-4.

[9] A. M. McDonald and M. A. van Wyk, "Efficient generation of random signals with prescribed probability distribution and spectral bandwidth via ergodic transformations," in *Proc. 26th Eur. Signal Process. Conf. (EUSIPCO)*, Rome, Italy, Sep. 2018, pp. 331–335, doi: 10.23919/EUSIPCO.2018.8553152.

[10] A. M. McDonald, M. A. V. Wyk, and G. Chen, "The inverse Frobenius–Perron problem: A survey of solutions to the original problem formulation," *AIMS Math.*, vol. 6, no. 10, pp. 11200–11232, Aug. 2021, doi: 10.3934/math.2021650.

[11] S. Grossmann and S. Thomae, "Invariant distributions and stationary correlation functions of one-dimensional discrete processes," *Zeitschrift für Naturforschung A*, vol. 32, no. 12, pp. 1353–1363, Dec. 1977, doi: 10.1515/zna-1977-1204.

[12] A. Baranovsky and D. Daems, "Design of one-dimensional chaotic maps with prescribed statistical properties," *Int. J. Bifurcation Chaos*, vol. 5, no. 6, pp. 1585–1598, Dec. 1995, doi: 10.1142/s0218127495001198.

[13] X. Nie and D. Coca, "A new approach to solving the inverse Frobenius–Perron problem," in *Proc. Eur. Control Conf. (ECC)*, Zurich, Switzerland, Jul. 2013, pp. 2916–2920, doi: 10.23919/ECC.2013.6669502.

[14] X. Nie and D. Coca, "Reconstruction of one-dimensional chaotic maps from sequences of probability density functions," *Nonlinear Dyn.*, vol. 80, no. 3, pp. 1373–1390, May 2015, doi: 10.1007/s11071-015-1949-9.

[15] M. Magfirawaty, A. A. Lestari, A. R. A. Nurwa, M. T. Suryadi, and K. Ramli, "A novel discrete-time chaos-function-based random-number generator: Design and variability analysis," *Symmetry*, vol. 14, no. 10, p. 2122, Oct. 2022, doi: 10.3390/sym14102122.

[16] M. Lawnik, A. Banasik, and A. Kapczyński, "Generation of values from discrete probability distributions with the use of chaotic maps," *Int. J. Comput.*, vol. 19, no. 1, pp. 49–54, Mar. 2020, doi: 10.47839/ijc.19.1.1692.

[17] M. Lawnik, "Generation of pseudo-random numbers from given probabilistic distribution with the use of chaotic maps," in *Proc. AIP Conf.*, vol. 1926, Jan. 2018, pp. 1–6, doi: 10.1063/1.5020474.

[18] M. Lawnik, "Generation of pseudo-random numbers with the use of inverse chaotic transformation," *Open Math.*, vol. 16, no. 1, pp. 16–22, Feb. 2018, doi: 10.1515/math-2018-0004.

[19] M. Pätzold, *Mobile Radio Channels*, 2nd ed., Chichester, U.K.: Wiley, 2012, doi: 10.1002/9781119974116.

[20] L. Zeng, X. Cheng, C.-X. Wang, and X. Yin, "A 3D geometry-based stochastic channel model for UAV-MIMO channels," in *Proc. IEEE Wireless Commun. Netw. Conf. (WCNC)*, San Francisco, CA, USA, Mar. 2017, pp. 1–5, doi: 10.1109/WCNC.2017.7925794.

[21] M. Salehi and E. Hossain, "On the effect of temporal correlation on joint success probability and distribution of number of interferers in mobile UAV networks," *IEEE Wireless Commun. Lett.*, vol. 8, no. 6, pp. 1621–1625, Dec. 2019, doi: 10.1109/LWC.2019.2932435.

[22] A. M. Mc Donald and J. C. Olivier, "A comparative study of deterministic and stochastic sum-of-sinusoids models of Rayleigh-fading wireless channels," in *Proc. IEEE Wireless Commun. Netw. Conf.*, Hong Kong, Mar. 2007, pp. 2027–2031, doi: 10.1109/WCNC.2007.380.

[23] K. Olivier, J. E. Cilliers, and M. Du Plessis, "Design and performance of wideband DRFM for radar test and evaluation," *Electron. Lett.*, vol. 47, no. 14, pp. 824–825, Jul. 2011, doi: 10.1049/el.2011.0362.

[24] J. J. Strydom, J. J. De Witt, and J. E. Cilliers, "High range resolution X-band urban radar clutter model for a DRFM-based hardware in the loop radar environment simulator," in *Proc. Int. Radar Conf.*, Lille, France, Oct. 2014, pp. 1–6, doi: 10.1109/RADAR.2014.7060264.

[25] J. J. Strydom, J. E. Cilliers, M. Gouws, D. Naicker, and K. Olivier, "Hardware in the loop radar environment simulation on wideband DRFM platforms," in *Proc. IET Int. Conf. Radar Syst. (Radar)*, Glasgow, U.K., Oct. 2012, pp. 1–5, doi: 10.1049/CP.2012.1687.

[26] J. J. Strydom, J. E. Cilliers, A. M. McDonald, and K. Olivier, "Hardware in the loop testing and evaluation of seaborne search radars," presented at the *Proc. 49th Annu. AOC Int. Conv. Symp.*, Phoenix, AZ, USA, Sep. 2012, pp. 1–30.

[27] J. J. Strydom and J. E. Cilliers, "Advances in the testing and evaluation of airborne radar through realtime simulation of synthetic clutter," in *Proc. 48th Annu. AOC Int. Conf. Symp.*, Washington, DC, USA, Nov. 2011, pp. 1–11.

[28] J. C. Smit, J. E. Cilliers, C. J. Baker, and J. J. Hanekom, "X-band high range resolution radar measurements of sea surface forward scatter at low grazing angles," in *Proc. IEEE Radar Conf.*, Rome, Italy, May 2008, pp. 1–4, doi: 10.1109/RADAR.2008.4721090.

[29] S. Watts, "Modeling and simulation of coherent sea clutter," *IEEE Trans. Aerosp. Electron. Syst.*, vol. 48, no. 4, pp. 3303–3317, Oct. 2012, doi: 10.1109/TAES.2012.6324707.

[30] K. D. Ward and S. Watts, "Use of sea clutter models in radar design and development," *IET Radar, Sonar Navigat.*, vol. 4, no. 2, pp. 146–157, Apr. 2010, doi: 10.1049/iet-rsn.2009.0132.

[31] P. Herselman, J. Cilliers, C. Baker, M. Greco, F. Gini, S. Watts, R. De Wind, and A. McDonald, "Evaluation and performance comparison of detection algorithms in a maritime environment," in *Proc. IEEE Radar Conf.*, Arlington, VA, USA, May 2010, pp. 920–925, doi: 10.1109/RADAR.2010.5494490.

[32] J. E. Cilliers, A. M. McDonald, J. J. Strydom, and M. A. van Wyk, "Hardware in the loop (HIL) generation of airborne clutter using a sum of complex sinusoids technique," in *Proc. IEEE Radar Conf. (RadarCon)*, Arlington, VA, USA, May 2015, pp. 1605–1609, doi: 10.1109/RADAR.2015.7131254.

[33] A. McDonald and J. Cilliers, "Arta process model of maritime clutter and targets," in *Proc. IET Int. Conf. Radar Syst. (Radar)*, Glasgow, U.K., Oct. 2012, pp. 1–6, doi: 10.1049/cp.2012.1671.

[34] L. Moysis, M. Lawnik, C. Volos, M. S. Baptista, and S. K. Goudos, "Chaotic maps with tunable mean value—Application to a UAV surveillance mission," *Symmetry*, vol. 15, no. 12, p. 2138, Dec. 2023, doi: 10.3390/sym15122138.

[35] M. A. Al-Mashhadani, "Random vibrations in unmanned aerial vehicles, mathematical analysis and control methodology based on expectation and probability," *J. Low Freq. Noise, Vib. Act. Control*, vol. 38, no. 1, pp. 143–153, Mar. 2019, doi: 10.1177/1461348418813031.

[36] M. A. Al-Mashhadani, "Optimal control and state estimation for unmanned aerial vehicle under random vibration and uncertainty," *Meas. Control*, vol. 52, nos. 9–10, pp. 1264–1271, Nov. 2019, doi: 10.1177/0020294019866860.

[37] M. S. Bartlett, *An Introduction to Stochastic Processes*, 2nd ed., Cambridge, U.K.: Cambridge Univ. Press, 1966.

[38] F. K. Diakonos, D. Pingel, and P. Schmelcher, "A stochastic approach to the construction of one-dimensional chaotic maps with prescribed statistical properties," *Phys. Lett. A*, vol. 264, nos. 2–3, pp. 162–170, Dec. 1999, doi: 10.1016/s0375-9601(99)00775-6.

[39] A. M. McDonald and M. A. van Wyk, "A novel approach to solving the generalized inverse Frobenius–Perron problem," in *Proc. IEEE Int. Symp. Circuits Syst. (ISCAS)*, Seville, Spain, Oct. 2020, pp. 1–5, doi: 10.1109/ISCAS45731.2020.9181115.

[40] A. McDonald and M. van Wyk, "Solution of the inverse Frobenius–Perron problem for semi-Markov chaotic maps via recursive Markov state disaggregation," in *Proc. 25th Eur. Signal Process. Conf. (EUSIPCO)*, Kos, Greece, Aug. 2017, pp. 1604–1608, doi: 10.23919/EUSIPCO.2017.8081480.

[41] A. McDonald and A. van Wyk, "Construction of semi-Markov ergodic maps with selectable spectral characteristics via the solution of the inverse eigenvalue problem," in *Proc. Asia–Pacific Signal Inf. Process. Assoc. Annu. Summit Conf. (APSIPA ASC)*, Kuala Lumpur, Malaysia, Dec. 2017, pp. 987–993, doi: 10.1109/APSIPA.2017.8282167.

[42] S. H. Isabelle, "A signal processing framework for the analysis and application of chaotic systems," Dept. Res. Lab. Electron., Massachusetts Inst. Technol., Cambridge, MA, USA, Tech. 593, 1995.

[43] A. M. McDonald, M. A. van Wyk, and G. Chen, "A direct solution to the stochastic inverse eigenvalue problem for complex-valued eigenspectra," *Linear Algebra Appl.*, vol. 658, pp. 262–282, Feb. 2023, doi: 10.1016/j.laa.2022.11.005.

[44] A. M. McDonald and M. A. van Wyk, "Identification of nonlinear discrete systems from probability density sequences," *IEEE Trans. Circuits Syst. I, Reg. Papers*, vol. 70, no. 2, pp. 846–859, Feb. 2023, doi: 10.1109/TCSI.2022.3219133.

[45] S. Sundaram and B. Gharesifard, "Distributed optimization under adversarial nodes," *IEEE Trans. Autom. Control*, vol. 64, no. 3, pp. 1063–1076, Mar. 2019, doi: 10.1109/TAC.2018.2836919.

[46] A. Lasota and M. C. Mackey, *Chaos, Fractals and Noise: Stochastic Aspects of Dynamics*, 2nd ed., New York, NY, USA: Springer, 1994, doi: 10.1007/978-1-4612-4286-4.

[47] G. D. Birkhoff, "Proof of the ergodic theorem," *Proc. Nat. Acad. Sci. USA*, vol. 17, no. 12, pp. 656–660, Dec. 1931, doi: 10.1073/pnas.17.2.656.

[48] P. Góra and A. Boyarsky, "A matrix solution to the inverse Frobenius–Perron problem," *Proc. Amer. Math. Soc.*, vol. 118, no. 2, pp. 409–414, Jan. 1993, doi: 10.1090/s0002-9939-1993-1129877-8.

[49] S. H. Isabelle and G. W. Wornell, "Statistical analysis and spectral estimation techniques for one-dimensional chaotic signals," *IEEE Trans. Signal Process.*, vol. 45, no. 6, pp. 1495–1506, Jun. 1997, doi: 10.1109/78.599984.

[50] G. Strang, *Linear Algebra and Its Applications*, 4th ed., Boston, MA, USA: Cengage Learning, 2006.

[51] X. Li, M. Yan, X. Zhang, M. Han, A. W.-K. Law, and X. Yin, "Efficient data-driven predictive control of nonlinear systems: A review and perspectives," *Digit. Chem. Eng.*, vol. 14, Mar. 2025, Art. no. 100219, doi: 10.1016/j.dche.2025.100219.

[52] M. Korda and I. Mezić, "Linear predictors for nonlinear dynamical systems: Koopman operator meets model predictive control," *Automatica*, vol. 93, pp. 149–160, Jul. 2018, doi: 10.1016/j.automatica.2018.03.046.

[53] J. Coulson, J. Lygeros, and F. Dörfler, "Data-enabled predictive control: In the shallows of the DeePC," in *Proc. 18th Eur. Control Conf. (ECC)*, Naples, Italy, Jun. 2019, pp. 307–312, doi: 10.23919/ECC.2019.8795639.

[54] A. Narasingam and J. S.-I. Kwon, "Application of Koopman operator for model-based control of fracture propagation and proppant transport in hydraulic fracturing operation," *J. Process Control*, vol. 91, pp. 25–36, Jul. 2020, doi: 10.1016/j.jprocont.2020.05.003.

[55] Y. Shi, X. Hu, Z. Zhang, Q. Chen, L. Xie, and H. Su, "Data-driven identification and fast model predictive control of the ORC waste heat recovery system by using Koopman operator," *Control Eng. Pract.*, vol. 141, Dec. 2023, Art. no. 105679, doi: 10.1016/j.conengprac.2023.105679.

[56] J. C. Schulze, D. T. Doncevic, and A. Mitsos, "Identification of MIMO Wiener-type Koopman models for data-driven model reduction using deep learning," *Comput. Chem. Eng.*, vol. 161, May 2022, Art. no. 107781, doi: 10.1016/j.compchemeng.2022.107781.

[57] Y. Xu, M. Netto, and L. Mili, "Propagating parameter uncertainty in power system nonlinear dynamic simulations using a Koopman operator-based surrogate model," *IEEE Trans. Power Syst.*, vol. 37, no. 4, pp. 3157–3160, Jul. 2022, doi: 10.1109/TPWRS.2022.3164585.

[58] J. Ge, Y. Xu, Z. Wu, L. Mili, S. Lu, Q. Hu, and W. Gu, "Data-driven optimal PMU placement for power system nonlinear dynamics using Koopman approach," *IEEE Trans. Ind. Informat.*, vol. 20, no. 9, pp. 11306–11317, Sep. 2024, doi: 10.1109/TII.2024.3399877.

[59] T. Zhao, M. Yue, and J. Wang, "Deep learning-based Koopman modeling for online control synthesis of nonlinear power system transient dynamics," *IEEE Trans. Ind. Informat.*, vol. 19, no. 10, pp. 10444–10453, Oct. 2023, doi: 10.1109/TII.2023.3240939.

[60] H. Chen, X. He, S. Cheng, and C. Lv, "Deep Koopman operator-informed safety command governor for autonomous vehicles," *IEEE/ASME Trans. Mechatronics*, vol. 29, no. 5, pp. 3568–3578, Oct. 2024, doi: 10.1109/TMECH.2023.3349052.

[61] H. Chen and C. Lv, "Incorporating ESO into deep Koopman operator modeling for control of autonomous vehicles," *IEEE Trans. Control Syst. Technol.*, vol. 32, no. 5, pp. 1854–1864, Sep. 2024, doi: 10.1109/TCST.2024.3378456.

[62] G. Mamakoukas, M. L. Castaño, X. Tan, and T. D. Murphey, "Derivative-based Koopman operators for real-time control of robotic systems," *IEEE Trans. Robot.*, vol. 37, no. 6, pp. 2173–2192, Dec. 2021, doi: 10.1109/TRO.2021.3076581.

[63] M. Han, K. Wong, J. Euler-Rolle, L. Zhang, and R. K. Katzschmann, "Robust learning-based control for uncertain nonlinear systems with validation on a soft robot," *IEEE Trans. Neural Netw. Learn. Syst.*, vol. 36, no. 1, pp. 510–524, Jan. 2025, doi: 10.1109/TNNLS.2023.3328643.

[64] F. Chen and W. Ren, "On the control of multi-agent systems: A survey," *Found. Trends Syst. Control*, vol. 6, no. 4, pp. 339–499, Jul. 2019, doi: 10.1561/2600000019.

[65] Y. Pan, W. Ji, H.-K. Lam, and L. Cao, "An improved predefined-time adaptive neural control approach for nonlinear multiagent systems," *IEEE Trans. Autom. Sci. Eng.*, vol. 21, no. 4, pp. 6311–6320, Oct. 2024, doi: 10.1109/TASE.2023.3324397.

[66] S. Yang, Y. Pan, L. Cao, and L. Chen, "Predefined-time fault-tolerant consensus tracking control for multi-UAV systems with prescribed performance and attitude constraints," *IEEE Trans. Aerosp. Electron. Syst.*, vol. 60, no. 4, pp. 4058–4072, Aug. 2024, doi: 10.1109/TAES.2024.3371406.

[67] S. V. Ershov and G. G. Malinetskii, "The solution of the inverse problem for the Frobenius–Perron equation," *USSR Comput. Math. Math. Phys.*, vol. 28, no. 5, pp. 136–141, Jan. 1988, doi: 10.1016/0041-5553(88)90022-5.

[68] N. Friedman and A. Boyarsky, "Construction of ergodic transformations," *Adv. Math.*, vol. 45, no. 3, pp. 213–254, Sep. 1982, doi: 10.1016/s0001-8708(82)80004-2.

[69] A. Rogers, R. Shorten, and D. M. Heffernan, "A novel matrix approach for controlling the invariant densities of chaotic maps," *Chaos, Solitons Fractals*, vol. 35, no. 1, pp. 161–175, Jan. 2008, doi: 10.1016/j.chaos.2006.05.017.

[70] A. Rogers, R. Shorten, D. M. Heffernan, and D. Naughton, "Synthesis of piecewise-linear chaotic maps: Invariant densities, autocorrelations, and switching," *Int. J. Bifurcation Chaos*, vol. 18, no. 8, pp. 2169–2189, Aug. 2008, doi: 10.1142/s0218127408021646.

[71] A. R. Rogers, "Synthesis and applications of chaotic maps," Ph.D. dissertation, Dept. Math. Phys., Nat. Univ. Ireland, Maynooth, Ireland, 2005.

[72] A. Rogers, R. Shorten, and D. M. Heffernan, "Synthesizing chaotic maps with prescribed invariant densities," *Phys. Lett. A*, vol. 330, no. 6, pp. 435–441, Oct. 2004, doi: 10.1016/j.physleta.2004.08.022.

[73] C. Fox, L.-J. Hsiao, and J.-E. Lee, "Solutions of the multivariate inverse Frobenius–Perron problem," *Entropy*, vol. 23, no. 7, p. 838, Jun. 2021, doi: 10.3390/e23070838.

[74] E. AlFarajat, "Invariant measures of random dynamical systems with constant probabilities," Ph.D. dissertation, Dept. Math. Statist., Concordia Univ., Montréal, QC, Canada, 2021.

[75] P. M. Uhl, H. Bohn, and N. H. Rhee, "On constructing chaotic maps with a prescribed probability distribution," *Missouri J. Math. Sci.*, vol. 30, no. 1, pp. 77–84, May 2018, doi: 10.35834/mjms/1534384957.

[76] H. Baik, A. Rafiqi, and C. Wu, "Constructing pseudo-Anosov maps with given dilatations," *Geometriae Dedicata*, vol. 180, no. 1, pp. 39–48, Feb. 2016, doi: 10.1007/s10711-015-0089-1.

[77] N. Wei, "Solutions of the inverse Frobenius–Perron problem," M.S. thesis, Dept. Math. Statist., Concordia Univ., Montréal, QC, Canada, 2015.

[78] J. A. Vargas and A. S. Argáez, "Rational maps of $\mathbb{P}^n$ with prescribed fixed points and the smooth conic case," *J. Algebra Appl.*, vol. 13, no. 8, Dec. 2014, Art. no. 1450066, doi: 10.1142/s0219498814500662.

[79] J. N. R. Daculio, R. N. Padua, and D. A. Tarepe, "Chaotic dynamical systems representation of seismic signals through inverse Frobenius–Perron," *Liceo J. Higher Educ. Res.*, vol. 16, no. 1, pp. 1–14, Jun. 2020, doi: 10.7828/ljher.v16i1.1364.

[80] N. Santitissadeekorn and E. M. Bollt, "Ensemble-based method for the inverse Frobenius–Perron operator problem: Data-driven global analysis from spatiotemporal 'movie' data," *Phys. D, Nonlinear Phenomena*, vol. 411, Oct. 2020, Art. no. 132603, doi: 10.1016/j.physd.2020.132603.

[81] X. Nie, D. Coca, J. Luo, and M. Birkin, "Solving the inverse Frobenius–Perron problem using stationary densities of dynamical systems with input perturbations," *Commun. Nonlinear Sci. Numer. Simul.*, vol. 90, Nov. 2020, Art. no. 105302, doi: 10.1016/j.cnsns.2020.105302.

[82] X. Nie, J. Luo, D. Coca, M. Birkin, and J. Chen, "Identification of stochastically perturbed autonomous systems from temporal sequences of probability density functions," *J. Nonlinear Sci.*, vol. 28, no. 4, pp. 1467–1487, Aug. 2018, doi: 10.1007/s00332-018-9455-0.

[83] X. Nie and D. Coca, "A matrix-based approach to solving the inverse Frobenius–Perron problem using sequences of density functions of stochastically perturbed dynamical systems," *Commun. Nonlinear Sci. Numer. Simul.*, vol. 54, pp. 248–266, Jan. 2018, doi: 10.1016/j.cnsns.2017.05.011.

[84] L. Ciampolini, S. Meignen, O. Menut, and T. David, "Direct solution of the inverse stochastic problem through elementary Markov state disaggregation," HAL Ouvertes, Lyon, France, Tech. Rep. Hal-01016804, Jul. 2014, pp. 1–12.

[85] M. T. Chu and G. H. Golub, *Inverse Eigenvalue Problems: Theory, Algorithms, and Applications*, 1st ed., Oxford, U.K.: Oxford Univ. Press, 2005, doi: 10.1093/acprof:oso/9780198566649.001.0001.

[86] Z. Zhao, Z.-J. Bai, and X.-Q. Jin, "A Riemannian inexact Newton-CG method for constructing a nonnegative matrix with prescribed realizable spectrum," *Numerische Math.*, vol. 140, no. 4, pp. 827–855, Dec. 2018, doi: 10.1007/s00211-018-0982-2.

[87] G. Steidl and M. Winkler, "A new constrained optimization model for solving the nonsymmetric stochastic inverse eigenvalue problem," *Linear Multilinear Algebra*, vol. 70, no. 18, pp. 3419–3448, Dec. 2022, doi: 10.1080/03081087.2020.1841077.

[88] M. Marcus and H. Minc, *A Survey of Matrix Theory and Matrix Inequalities*, 1st ed., New York, NY, USA: Dover, 1992.

[89] H. Perfect and L. Mirsky, "Spectral properties of doubly-stochastic matrices," *Monatshefte für Math.*, vol. 69, no. 1, pp. 35–57, Feb. 1965, doi: 10.1007/bf01313442.

[90] J. Banasiak, "Chaotic linear systems in mathematical biology," *South Afr. J. Sci.*, vol. 104, nos. 5–6, pp. 173–179, Jun. 2008.

ANDRÉ MARTIN MCDONALD (Member, IEEE) received the B.Eng., B.Eng. (Hons.), and M.Eng. degrees in computer and electronic engineering from the University of Pretoria, Pretoria, South Africa, in 2004, 2005, and 2010, respectively, and the Ph.D. degree in electronic engineering from the University of the Witwatersrand, Johannesburg, South Africa, in 2024.

In 2005, he was a Teaching Assistant with the Department of Electrical, Electronic and Computer Engineering, University of Pretoria. From 2009 to 2012, he was a Researcher with the Defence, Peace, Safety and Security Operating Unit, Council for Scientific and Industrial Research (CSIR), Pretoria. From 2012 to 2019, he was a Senior Researcher with the Modelling and Digital Science Operating Unit, CSIR. He is currently a Principal Researcher with the Defence and Security Cluster, CSIR. His research interests include dynamical systems, signal processing, and mathematical modeling.

MICHAËL ANTONIE VAN WYK (Senior Member, IEEE) received the B.Eng. and M.Eng. degrees in electrical engineering and the Ph.D. degree in applied mathematics from Rand Afrikaans University, Johannesburg, South Africa, in 1986, 1989, and 1996, respectively.

From 1987 to 1992, he completed his compulsory national service and worked in the aerospace industry. In 1992, he joined Rand Afrikaans University, as a Lecturer. He is currently a Full Professor and the Carl and Emily Fuchs Chair in systems and control with the School of Electrical and Information Engineering, University of the Witwatersrand, Johannesburg; and the Head of the Systems and Control Group. He has been appointed as an Adjunct Professor with the Department of Electrical Engineering, Nelson Mandela University, Port Elizabeth, South Africa. He has been a Consultant with the aerospace and electronic systems industry in the areas of signal processing and control, nationally and internationally. His current research interests include analysis and modeling of nonlinear dynamical systems and networks and algorithm development in signal and image processing.

JACQUES ÉTIENNE CILLIERS received the B.Eng. and M.Eng. degrees in electronic engineering from the University of Pretoria, Pretoria, South Africa, in 1994 and 2002, respectively, and the Ph.D. degree in information theory applied to radar target recognition from University College London (UCL), London, U.K., in 2018.

From 1997 to 1998, he was with Kentron, a division of Denel Aerospace, designing small target detection algorithms for imaging infra-red air-to-air missiles. From 1998 to 1999, he was with the Laboratory for Advanced Engineering (LGI), University of Pretoria, developing high speed, spectrally efficient digital modulation techniques and adaptive equalization algorithms for bit speeds up to 80 Mb/s over wireless channels. From 1999 to 2023, he was with the Defence and Safety (D&S) Operating Unit, Council for Scientific and Industrial Research (CSIR), Pretoria, as a Principal System Engineer and Signals/Systems Analyst in the field of radar and electronic warfare. From 2023 to 2024, he was with Tawazun Technology and Innovation (TTI), United Arab Emirates, as a Radar and EW Research and Development Specialist and has recently joined the Radar and EW Centre of Excellence (REW COE), EDGE Group. His research interests include adaptive signal processing, radar signal processing, array signal processing, multiple input multiple output (MIMO) radar, tracking radar, radar cross section (RCS) calculation, detection of small targets imbedded in sea clutter, clutter modeling, hardware in the loop (HIL) testing of radars, and radar-based target recognition.